_ TELECOM ESCUELA TÉCNICA VLC SUPERIOR DE UPV INGENIEROS DE TELECOMUNICACIÓN

UNIVERSITAT POLITÈCNICA DE VALÈNCIA

Absorción saturable de grafeno para láser mode-locked

Miguel Montesinos Ballester

Tutor: Pablo Sanchis Kilders

Cotutores: Bart Kuyken
Koen Alexander
Dries Van Thourhout

Trabajo Fin de Máster presentado en la Escuela Técnica Superior de Ingenieros de Telecomunicación de la Universitat Politècnica de València, para la obtención del Título de Máster en Ingeniería de Telecomunicación

Curso 2016-17

Valencia, 4 de julio de 2017

Acknowledgements

I would like to thank Prof. Dries Van Thourhout and Prof. Pablo Sanchis Kilders for their administrative and academic support during my exchange programme at the Photonics Research group of Ghent University.

I would also like to express profound gratitude towards my daily supervisors Prof. Bart Kuyken and Koen Alexander, who have not only been patient and tolerant to my quest in seeking knowledge, but also generous in sharing his expertise, immense knowledge and experience in this field of photonics. This thesis would not have been materialized without their help and guidance.

My personal full-hearted appreciation also goes to my family, who have brought me the possibility of this exchange.

Resumen

Desde la primera exfoliación del grafeno monocapa en 2004, la investigación sobre este material 2D ha aumentado exponencialmente. El grafeno, una capa bidimensional de átomos de carbono dispuestos en una red hexagonal que se comporta claramente diferente al resto de materiales 3D. El grafeno no sólo tiene propiedades mecánicas únicas, este material también tiene extraordinarias propiedades eléctricas y ópticas, debido principalmente a su sistema de bandas lineal y sin separación entre ellas (cero “bandgap”). Además, este material permite una fuerte interacción luz-materia, que puede ser explotada para la detección de luz o modulación. Asimismo, debido a esta fuerte interacción, se ha observado que una vez que la intensidad óptica alcanza un cierto umbral, aparece una saturación en la absorción de luz. Este fenómeno puede ser explotado para la implementación de láseres de bloqueo de modo, una técnica utilizada para producir pulsos de luz coherente y extremadamente cortos.

El grafeno ya se ha utilizado con éxito para la implementación de láseres con bloqueo de modos en fibra, sin embargo, también se puede utilizar para la fabricación de láseres a escala de chip con pulsos de femtosegundos, mediante su deposición en guías integradas de silicio. Los investigadores de UGent (en estrecha colaboración con Imec) han estado trabajando en la integración del grafeno en estructuras fotónicas basasdas en Silicio sobre aislante (“Silicon-on-Insulator”). Este grupo de investigación ya ha demostrado experimentalmente una absorción saturable eléctricamente sintonizable, que puede ser utilizada para realizar láseres con bloqueo de modos espontáneo integrados y con una duración de pulso eléctricamente sintonizable, haciendo que el sueño de un láser de femtosegundos a escala de chip casi una realidad.

El objetivo de esta tesis es demostrar el mismo fenómeno de absorción saturable eléctricamente sintonizable, pero sobre guías de ondas de nitruro de silicio, que evita el efecto de absorción de dos fotones en las longitudes de onda de telecomunicaciones debido a su mayor “bandgap”. Este efecto es fuerte en las guías de onda de silicio, y limita la cantidad de potencia que puede propagarse en los enlaces ópticos.

Resum

Des de la primera exfoliació del grafè monocapa el 2004, la investigació sobre aquest material 2D ha augmentat exponencialment. El grafè, una capa bidimensional d'àtoms de carboni disposats en una xarxa hexagonal que es comporta clarament diferent a la resta de materials 3D. El grafè no només té propietats mecàniques úniques, aquest material també té extraordinàries propietats elèctriques i òptiques, a causa principalment del seu sistema de bandes lineal i sense separació entre elles (zero "bandgap"). A més, aquest material permet una forta interacció llum-matèria, que pot ser explotada per a la detecció de llum o modulació. Així mateix, a causa d'aquesta forta interacció, s'ha observat que una vegada que la intensitat òptica arriba a un cert llindar, apareix una saturació en l'absorció de llum. Aquest fenomen pot ser explotat per a la implementació de làsers de bloqueig de modes, una tècnica utilitzada per produir polsos de llum coherent i extremadament curts.

El grafè ja s'ha utilitzat amb èxit per a la implementació de làsers amb bloqueig de modes en fibra, però, també es pot utilitzar per a la fabricació de làsers a escala de xip amb polsos de femtosegons, mitjançant la seva deposició en guies integrades de silici. Els investigadors de UGent (en estreta col·laboració amb Imec) han estat treballant en la integració del grafè en

estructures fotòniques basasdas en Silici sobre aïllant ("Silicon-on-Insulator"). Aquest grup de recerca ja ha demostrat experimentalment una absorció saturable elèctricament sintonitzable, que pot ser utilitzada per realitzar làsers amb bloqueig de modes espontani integrats i amb una durada de pols elèctricament sintonitzable, fent que el somni d'un làser de femtosegons a escala de xip siga quasi una realitat.

L'objectiu d'aquesta tesi és demostrar el mateix fenomen d'absorció saturable elèctricament sintonitzable, però sobre guies d'ones de nitrur de silici, que evita l'efecte d'absorció de dos fotons en les longituds d'ona de telecomunicacions a causa del seu major "bandgap". Aquest efecte és fort en les guies d'ona de silici, i limita la quantitat de potència que pot propagar-se en els enllaços òptics.

Abstract

Since the first successful exfoliation of monolayer graphene in 2004, research interest in this 2D material has surged exponentially. Graphene, a two dimensional layer of carbon atoms arranged in a hexagonal lattice, behaves distinctly different from regular 3D materials. Not only does graphene have unseen mechanical properties, the material also has extraordinary electrical and optical properties, mainly originating from its linear and gapless band structure. Moreover, this material allows for a strong light-matter interaction, which can be exploited for light detection or modulation. Furthermore, due to this strong interaction, it has been observed that once optical intensity reaches a certain threshold saturable absorption takes place. This phenomenon can be exploited for mode locking lasers, a technique used to produce extremely short and coherent light pulses.

Graphene has already been successfully used for mode locking fiber lasers, however it can also be used to make chip scale femtosecond lasers by depositing it on integrated silicon waveguides. Researchers at UGent (in close cooperation with Imec) have been working on the integration of graphene with photonic structures on a Silicon-on-Insulator waveguides and they have experimentally demonstrated electrically tunable saturable absorption, which can be used for realizing integrated spontaneously mode locked lasers with an electrically tunable pulse duration, making the dream of a ultrashort chip scale femtosecond laser almost a reality.

The objective of this thesis is to demonstrate the same phenomenon, but on top of a Silicon Nitride waveguide instead of SOI, which avoids the two-photon absorption effect at telecom wavelengths due to its larger bandgap. This effect is strong in SOI waveguides, where it limits the amount of power than can propagate in the photonic wires.

Index

1. Introduction

1.1. Mode-locked Lasers

Ultrashort pulsed lasers, producing pulses with pulse lengths on the order of femtoseconds, have become more and more important in the current research community [1]. Optical frequencies [2, 3], atomic and molecular spectra, lengths, distances [4], and displacements [5] are commonly measured with this kind of laser. Furthermore, they are nowadays also used to achieve in-vivo 3D imaging of the human retina, epidermis, and blood vessels [10]. Optical frequency combs produced by femtosecond lasers are also used to probe and manipulate the quantum state of gaseous atoms and molecules [11], and in all forms of condensed matter [12]. They are also used in astrophysics equipment, for example, to calibrate spectrometers with an incredible accuracy that allows for scientists to measure Doppler shifts of stellar objects with an error of about 1 cm/s [13, 14, 15]. Moreover, in the near future, fs-lasers could be used for timing synchronization in large particle accelerators [16]. The most common way to achieve a fs-laser is using passively mode-locked lasers with saturable absorbers [6, 7, 8, 9].

Stable ultrafast optical pulses are obtained from mode locked lasers. The simplest form is a pair of mirrors that only allows a half-integer number of wavelengths in an inside standing wave. The wave (or mode) number is the number of wavelengths in a specific standing wave. The gain crystal of the laser affects the number of allowed modes in the cavity. A certain number of waves allowed by the gain crystal and the cavity length can coexist without mode-locking and a constant out intensity. It is because their relative phase oscillates, but if the relative phase is fixed a mode-locked has been reached. It means that all these waves interfere constructively at regular intervals causing extremely short and high intensity pulses, while interferes destructively each other at the rest of time [53].

Furthermore, a mode locked laser can be made by putting a saturable absorber inside the cavity, allowing for absorption at low intensities. If the laser is not mode locked, the light fluctuates semi-randomly because of the constructively and destructively interferences between allowed waves. But if a saturable absorber is places into the cavity, the lower fluctuation will be absorbed at each round trip while high intensities pass through the saturable absorber with small loss. Due to this optical intensity dependence and the subsequently high intensity contrast, light begins to operate in the pulsed state.

Figure 1 shows how a saturable absorber attenuates more the low intensities than higher ones, narrowing the pulses iteration by iteration. The width of these pulses depends on the gain and

bandwidth of the material as well as to the response time of the saturable absorber. As more modes are allowed inside the cavity, narrower pulses could be achieved. In the same way, as a faster saturable absorber is used, shorten pulses are reached.

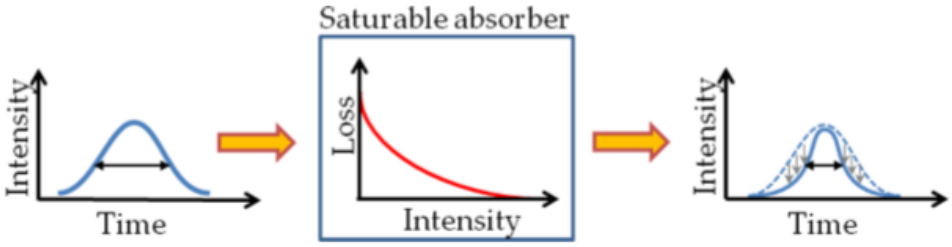

Figure 1. How saturable absorber affects to a pulse shape [53].

1.2. Saturable absorber

A saturable absorber can be described as a device that has low losses for high light intensity and higher losses for lower intensities. It can be thought as a material of which the absorption saturates at certain intensity causing a decrease in the losses.

The firsts saturable absorbers were made in 70s and 80s, mode-locking was achieved without Q-switching instabilities integrating them in dye lasers. This method was first demonstrated by Shank and Ippen in 1974 [18], who obtained a pulse width of 0.5 – 1.0 ps by putting a couple of saturable absorbers and a gain medium of a single-free dye stream in the centre of the laser resonator [18]. Later, in 1976 Rudlock and Bradley got pulses of 0.3 ps using a similar approach, but only 5 year later Fork et al. [19] achieved the first sub-100 fs-laser. To get these ultra-short pulses, they implemented a mode locked dye laser using the interaction of two synchronized counter propagating pulses together with a thin saturable absorber. Despite all these reports, the technology used so far was not suitable to implement the best locked lasers because dye lasers have some important deficiencies, for example, these kind of lasers have a very short lifetime because of their high cross section gain [20].

As we can deduct from all this progress, the design of a mode locked laser, and specifically an artificial saturable absorber, caused a great interest in the scientific community. Thus, a new design was proposed in 1989 by Mark et al. [21] and Ippen et al. [22] in order to achieve shorter pulses. This new design was called additive pulse mode locking (APM) and makes use of the first artificial saturable absorber. An external cavity based on a single-mode fiber which is coupled to the laser cavity and has the same round trip. That way, the pulses from both cavities interfere at the coupling mirror such that they interfere constructively at the pulse centre and

destructively at the tails. In this manner, we can get narrower pulses. This effect is caused by the nonlinear phase shift that occurs in single mode fiber which is induced by the Kerr effect. This phase shift is larger at the temporal pulse centre, compared to both tails. Despite some papers having reported this method making mode locked lasers [23-25], it is quite difficult to achieve the same round trip in both external and main cavities. But, not only a high accuracy in adjusting the cavity lengths is needed, they must be interferometrically stabilized, too. These requirements make this technique a difficult challenge to achieve.

Later, in 1991, Spence et al. [26] improved the state-of-the-art artificial saturable absorbers with the invention of Kerr lens mode locking (KLM), used to generate pulses with a duration below of 10 ps. To implement this method, a nonlinear self-focusing effect is generated on the laser beam by using an active medium with Kerr nonlinearity. This Kerr effect can be described as the refractive index dependence on the light intensity. This active medium will act as a lensing device with an intensity dependent focusing power because of the gradients generated across the transverse mode profile in the gain medium. Thus, the Kerr effect becomes more important for this method than for others. This technique can be done in two different ways: soft aperture KLM and hard aperture KLM. In the first one, the Kerr lens reduces the beam radius in the gain medium and gives a better spatial overlap between the pump beam and the pulses, providing greater effective gain for the short pulses. For hard aperture KLM, the beam radius is also reduced by the Kerr lens but at the opening of the aperture, causing a reduction of the optical losses of short pulses [20]. This method has been investigated extensively, see references [27-36]. With KLM technique pulse widths of 5.4 femtoseconds has been achieved in a Ti:sapphire laser with no external cavity pulse compression [29]. Despite that we can get ps mode locked pulses with the APM technique, KLM is definitely more convenient because there is no cavity stabilization needed. Nevertheless, KLM has some huge disadvantages such as difficulty in getting the mode locking self-starting process or the accuracy needed in the cavity aligning close to its stability limit to have a stable pulse operation. This causes limitations in the cavity designs and becomes more critical the more average output power and more massive cavities there are [20].

Due to the increasing interest in saturable absorbers, another kind of device appeared as an alternative to KLM, the semiconductor saturable absorber mirrors (SESAMs). The first SESAMs were reported by Keller et al. [37] in 1992, implemented in a Nd:YLF laser. This device has some important advantages such as self-starting or pure continuous wave passive mode locking without presenting any Q-switched instabilities. This invention aroused the interest of the scientific community and many other new designs of SESAMs were developed.

The current SESAMs work as an intra-cavity saturable absorber and are based on a set of non-absorbing semiconductor layers grown on a Bragg semiconductor mirror, with quantum wells or bulk absorber enclosed between layers. This design, which mixes semiconductor layers and Bragg mirror, provides a Fabry-Perot structure [20]. Although with previous saturable absorbers was not possible, with SESAMs it became possible to set the linear and nonlinear optical properties by taking advantage of the already developed semiconductor growth technology and bandgap engineering. With these mature technologies the researchers are able to control all parameters of the SESAM, such as the wavelength, saturation fluence recovery time, absorber lifetime, modulation depth or saturation intensity. This almost absolute control of all parameters allows the researchers to implement pure passively Q-switched lasers, achieving pulses duration from microseconds to nanoseconds, or mode locked pulsed lasers with pulse durations from picoseconds to femtoseconds [38]. Moreover, as the SESAMs are so compact, the insertion losses introduced are quite low.

As a result, nowadays SESAMs are one of the most common devices to get mode locked pulses with an operational wavelength from 800 to 1550 nm and the best results have been reported with multi-quantum wells (MQWs) SESAMs, which are implemented with III-V group binary and ternary elements [39-43]. The common method used for growing the SESAM on the Bragg reflector can be either molecular beam epitaxy (MBE) or metal-organic vapour phase epitaxy (MOVPE) [39, 44-46]. The design of these devices has been developing during the last 20 years and, in order to improve the achievements in ultrashort pulses generation, many researches have reported in this area [38, 40-52].

Despite all their advantages, SESAMs have some handicaps. The optical damage threshold is low, so if the output pulse repetition rate is increased to high levels, this device is easily damaged and therefore its functional life expectancy is reduced [53, 54]. Another weak point of the SESAMs is the dependency of the minimum output pulse width on the carrier relaxation time of the absorber, that fact limits the pulse width engineering [53]. The complexity and cost of fabrication of these devices is another important drawback. Moreover, in its fabrication the process of high-energy heavy-ion implantation is used, this can cause some imperfections when decreasing the recovery time to picosecond scale. Also, after fabrication, it is quite difficult to remove this device from the crystalline substrate on which it has been grown, which also causes difficulties.

When designing and integrating fiber-based SESAMs it is highly important to be compatible with fiber optic lasers, but when a larger size or higher saturation intensity than common SESAMs is

desired, this compatibility can be achieved but the output can be unstable. Moreover, the fiber-based SESAMs are polarization dependent, that is usually undesired [55], and the wavelength tunability depends on the resonant nonlinearity, so that the wavelength range of operation is limited to a few nanometres [39-41, 45, 56-58] and is not suitable for broadband tunable pulse generation [59, 60].

After these achievements, demand of these kind of devices increased and the development of better saturable absorbers with new materials that enhanced their properties became necessary, such as wider wavelength range, simplicity, a reduction of the fabrication cost or easy packaging, always with strong ultrafast optical nonlinearities [39].

While these SESAMs were developed, a new group of carbon materials were discovered, they are broadly known as carbon nanotubes (CNTs). This new material is basically a 1-D cylindrical structure of about 1 μm length and from 0.6 to 2 nm of diameter. The properties of these materials allows for getting beyond most of the previous technology (e.g., SESAMs) disadvantages, they can be simultaneously introduced in fiber-based devices and also in a simple way.

There are many different ways to generate CNTs, among we can find laser vaporization [61], metal-catalysed disproportionation of carbon monoxide [62], arc discharge [63] or gas-phase pyrolysis [64]. With all these processes it is possible to get mass production of CNTs, which reduces the fabrication cost of the material [65]. It is also possible to implement fiber-end method, embedding CNTs into fiber-based optical lasers [66]. This technique can be done by putting a thin film of this polymer between two ferrules [67-70] or by direct synthetization and depositing of CNTs [65, 71-72]. Depending on the kind of structure this technology can be divided in two different classes: single walled carbon nanotubes (SWCNTs) and multi-walled carbon nanotubes (MWCNTs). As the single walled type is based in only one single cylinder, it has more singular optical properties compared to multi-walled nanotubes [65].

Compared to the previous saturable absorbers based on semiconductors (SESAMs), the most important advantages that this new technology brought to the scientific community were an inherently fast saturable absorption [55, 72, 73] together with a fast recovery time, typically less than 1ps [65], making it ideal to generate ultrashort pulse mode locked lasers [55]. But another important advantage is broad wavelength range, which starts from near infrared up to UV [39, 74, 75]. This phenomenon is due to the bandgap properties of CNTs, where each synthetized nanotube has a certain radius or symmetry and therefore a different absorption bandgap [65]. This bandgap is estimated as inversely proportional to its diameter. [39, 76].

In this way, the light is absorbed by the CNTs whose bandgap matches with the incident light energy and, as there is a wide range of CNTs diameters, the absorption wavelength range can be wide too. In other words, the CNTs absorption is determined by the bandgap energy, which is also dependent on the diameter of the CNTs [77]. Trying to use this phenomenon, many researches have been done to achieve tunable mode-locked fiber lasers based on carbon nanotubes [60, 78-80].

But these saturable absorbers based on CNTs are not perfect, they have some drawbacks. For example, they have a wide wavelength range which is important for tunable applications, but this also leads to extra insertion losses due to the CNTs of different bandgap [77, 81]. The extra linear absorption caused by the unused CNTs causes some difficulties to reach mode locked operation state. Another weakness is that CNTs tend to stack, what causes some scattering at these points [81] and deteriorates the mode locked laser behaviour. Hence, a novel material which solves these shortcomings became needed.

Aside from carbon nanotubes, another carbon allotrope is Graphene, which has been widely researched and used in many applications, among others as saturable absorbers for broadband ultrafast lasers. It is heavily expected that Graphene will replace CNTs, SESAMs or any other kind of the previous technology [17]. Graphene is basically a single layer of carbon atoms forming a 2-D net with hexagonal pattern. Due to its configuration and the links between atoms, this novel material has many extraordinary properties, not only in photonics but also in optoelectronics, chemistry, material science, space or even in biology [17].

The term “graphene” was used for first time in 1987 by Mouras et al. to describe a single sheet of graphite as one of the constituents and the IUPAC (International Union of Pure and Applied Chemistry) commission later replaced the term “graphite layers” with “graphene”. But a high quality single layer of graphene could not be achieved until 2004 [82], by Andre Geim and Kostya Novoselov and with which they got the Nobel Prize in 2010 [53]. According to the current definition, graphene is a 2-D monolayer of carbon atoms, which is the basic building block of graphitic materials such as fullerene, carbon nanotubes, graphite, etc. [17]

The photo-excited carrier dynamics, and thus the saturable absorption [83], in graphene is related to Pauli blocking as illustrated in [77]. As we can see in the literature, graphene offers many interesting and useful properties that make this material a useful saturable absorber [53, 77, 84-92]. One of these properties is the linear dispersion of Dirac electrons, this means that an electron-hole pair always exist for any excitation energy. It is caused by its gapless condition and provides a broad absorption which can be useful for broadband pulsed generation [77, 93] and

so the saturable absorption becomes independent to the wavelength [90, 94, 95]. Another interesting property of graphene is its ultrafast carrier dynamics [77, 96-98] which makes it so convenient for ultra-short and pulse generation lasers with high repetition rate [53, 101, 102], together with a large absorption of incident light per layer [77, 99, 100]. All these extraordinary properties make graphene a material to be potentially used for passively mode locked [81, 86, 90] and Q-switched lasers [103, 104] with a wide wavelength range.

Compared with SESAMs or CNTs, graphene has the advantage of not requiring bandgap engineering to enhance the saturable absorber behaviour [77]. Also, this material has a broader wavelength range than SESAMs or CNTs.

Hence, graphene combines interesting characteristics related to saturation intensity, modulation depth, recovery time, saturation power and optical damage threshold and saturation fluence. All these unique properties required for a good saturable absorber makes that graphene will likely overthrow SESAMs and CNTs, overcoming their shortcomings [77].

Many ways to produce graphene have been successfully developed, from simple processes for small scale samples to complex methods for large scale production. The first process introduced was micromechanical exfoliation of graphite [105], which achieves the purest graphene with lowest defects. Nevertheless, it is impossible to use this method to produce large scale samples. But more complex methods have been developed to provide large areas, providing a firm supply of this material, such as Chemical Vapour Deposition (CVD) [106-109] or liquid phase exfoliation [110-112]. Moreover, graphene can be also produced by chemical synthesis [113, 114] and, as for CNTs, it is possible to integrate graphene in optical fiber systems making use of end-type methods.

1.3. Materials

For the implementation of a saturable absorber, the material used on it should be possible to be integrated in a common CMOS chip, in order to safe as much space as possible, as well as make profit of this mature technology and reduce the costs, too. The main material used in CMOS technology is Silicon. This material has been already used for saturable absorption in graphene [107]. But in order to achieve a broaden wavelength range, the chosen material in this Thesis for the waveguides has been Silicon Nitride, which can also be integrated in a chip and avoids the Two Photon Absorption effect in telecom wavelengths, due to its larger bandgap.

Due to its suitable properties above mentioned, the material chosen on this Thesis to achieve the saturable absorption effect has been graphene.

1.3.1. Silicon Nitride

Nonlinear silicon photonics is drawing a lot of interest due to its potential applications in telecommunications and spectroscopy. The nonlinear parameter of silicon has been reported to be up to five orders of magnitude higher than for standard optic fibers, because of its intrinsically high nonlinear index and the high confinement offered in silicon-on-insulator platform. However, the telecom band lies below half of the bandgap of silicon, thus the two photon absorption (TPA) takes relatively high values. Also, as the recombination time in silicon is relatively slow, about 1 nanosecond, the subsequent free carrier absorption (FCA) disturbs the measurements of most nonlinear effects.

Therefore, it is interesting to find the solution to overcome these drawbacks. The current ways taken in account are testing new materials compatible with common silicon platforms, taking out the carriers electrically and by using short pulses as the free carrier absorption becomes too low to have any influence.

It is possible to make use of hydrogenated amorphous silicon waveguides, of which measured bandgap, is 1.6 eV, whereas for crystalline silicon it is 1.12 eV. Such bandgap matches with a wavelength of 1550 nm for the two-photon-absorption threshold and for that reason parametric amplification up to 26.5 dB at telecom wavelengths has been demonstrated [115]. But at such high optical powers the material degrades due to the Staebler-Wronski effect or, in other words, the recombination of carriers.

As it is said before, there are known ways to overcome these problems. In order to reduce the TPA in these waveguides it is possible to increase the bandgap by doping the amorphous silicon with carbon. Another way could be to use another material with larger bandgaps such as III-V semiconductors, which can also be integrated in common silicon platforms (e.g. through bonding) and have similar high third order nonlinearities. Moreover, it is possible to overcome FCA by using short pulses [115]. Supercontinuum generation through soliton fission at telecom wavelengths also has been demonstrated. However, as FCA deteriorates the performance much more than TPA, it can be demonstrated that the continuous wave nonlinear effects could be detected if carriers are removed by integrating a reverse biased PIN junction.

Unlike other research that has been done in silicon, in this thesis these problems will be avoided by making use of Silicon Nitride, which has a bandgap of 5 eV. In that way we can avoid FCA as well as TPA, getting a wider working wavelength range than for (amorphous) silicon or doped-silicon.

1.3.2. Graphene

Graphene has been considered as an extraordinary material because of both uniquely linear and nonlinear optical properties, as well as having outstanding thermal, mechanical and electronic properties. Also, due to its gapless band structure graphene has been considered a favourable material for broadband optoelectronic applications, such as saturable absorber with ultrafast recovery time. Unlike any other material on earth, graphene has a zero bandgap, which allows electrons to migrate from valence to unoccupied conduction band (and vice-versa) freely. It is even more promising since it is possible to tune its optical transparency by shifting the Fermi level, achieving a tunable absorption together with a low insertion losses. In fact, a graphene based electro absorption modulator with low insertion losses has been experimentally demonstrated in [125], developed on SOI at the typical telecom wavelength of 1550 nm, getting similar properties as silicon Mach-Zehnder interferometer modulators. But not only for modulators is graphene useful, this material can be also used for ultrafast pumped lasers such as in Ref. [116]. Another great advantage is its compatibility with current CMOS technology, which leads to cheap designs and fabrication.

1.4. The Aim

Saturable absorption of graphene integrated on SOI has been demonstrated [119], but not on Silicon Nitride. The aim of this thesis is to demonstrate the electrical tunability of graphene absorption in SiN, which avoids the drawback of TPA on silicon. This electrical tunability will allow a more control in the saturable absorption properties. If demonstrated, this kind of saturable absorbers would lead to more broadband devices in many applications, such as modulators or pulsed laser as mentioned above.

2. General Background

2.1. Band Level System

To understand how saturable absorption works on semiconductors, it is first needed to understand its physics behaviour, specifically that according to quantum physics. This law says that electrons only can stay in particular states of material with certain energies. In most systems there are so many states that it can be approached to a continuum of states of energies allowed. Unlike in some conditions or materials they can touch each other, the difference between these energy levels where electrons cannot be present are called bandgaps [120]. Moreover, most of these bandgaps are so large that any electron would go to that levels, they just would go outside the entirely material. Thus, in practically all cases, only the two lowest levels will be taken in

account. The lowest energy band is called “valence band” and the second higher level is called “conduction band”. The space between these bands represents the set of momentums that correspond to the primitive unit cell for crystal in real space by Fourier Transform. The origin of this gap has an associated momentum usually called “Γ” and that point is also called “gamma point” [120]. On the other hand, the point with highest energy in the valence band is called “K” point and its associated momentum is usually named as “K”. The energy related to K point is also called “Dirac point”, but unless it is broadly known with this name, it is not the stander notation. Moreover, the Brillouin zone is defined as the inverse of the distance of the crystal, while the gap is defined by how strong the perturbation is of the lattice on the electrons.

As its name indicate, these bands are closely related with the material conductivity. In this way electrons are called as fermions and the Pauli exclusion principle only allow one electron in exactly the same quantic state or, in order words, the same point of band level. The fermion (or electron) of the highest level is in at the highest “Fermi level”, or also named “Fermi energy”. This level is where there is 50% probability of being occupied by the highest electron, but when this thesis talks about Fermi level refers to highest Fermi level. As more fermions are added to the system, the Fermi level increases more and more. But once the Fermi level reaches the conduction band and is at the K level (if there are not any overlap between bands), there are not empty states in valence band where an electron can fit, unless it reaches the next band, which is at too much energy compared to single electron energy to break that bandgap. If it happens, means that there is no place for another electron and thus any current can flow through the material, even if a voltage V is applied. In this cases, this material is called “insulator” or that it is in a “insulating phase” [120].

On the other hand, if the Fermi level is only near but above the conduction band, there are many places where the free electrons can be carried by applying certain voltage and thus a current flow can be achieved. If the material gets this state is said that it has reached an “electron conducting state” [53]. However, if the Fermi level is below the conduction band and is near the valence band, if an electron is excited it only has a few places to go, compared to if the Fermi level were near the conduction band. Thus, a “hole” (or lack of electron) appeared, which can be filled by any other electron, which in turn provoke another hole where it was. In consequence, if a certain voltage is properly applied, a current of holes can flow through the material. As these holes are actually an absence of electrons, they carry a positive charge and a material in this state is said that is in a “hole conduction phase” [53]. Also, as far the Fermi level is from the conducting band, higher conductivity the material has, because more holes there are to conduct.

Doing an analogy with the traffic on a highway, if the Fermi level is at the K point it means that all electrons are stuck in their own states because there is any place to move, as traffic jam where all the cars are in the same position because there is not any space to move, and therefore the material becomes an insulator (Figure 2.B). But if the Fermi level is in the conduction band, the material is in an electro-conducting phase and the electrons have many states where they can move if gets perturbed, this is kind of the same as an empty highway, where the cars con move with no retentions. (Figure 2.A) Finally, if the Fermi level is below the K point, near the valence band, electrons have a few spaces to move because the different states are almost full. In this way, holes (or empty spaces) can travel through the material (which is in a hole-conducting phase) under an applied field. It is similar as a busy highway were there are some spaces that are filled by cars, and it seem like these empty spaces are moving through the highway (Figure 2.C). The cars are moving quite slowly, but this empty space moves quickly in the opposite direction.

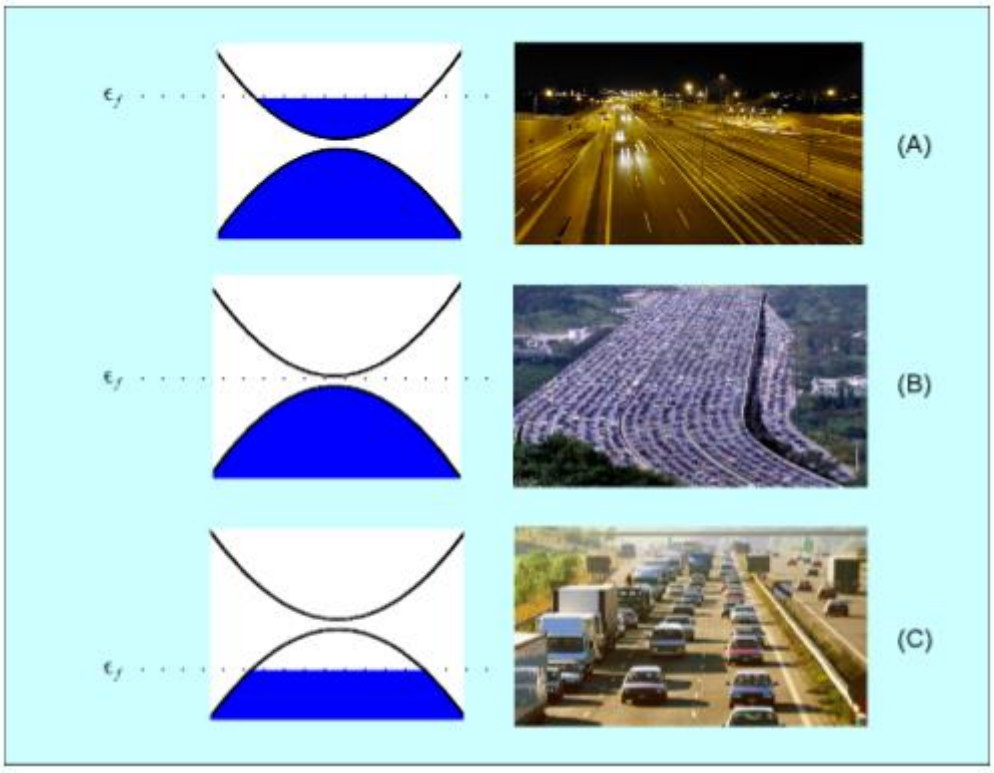

Figure 2. Different conduction phases as analogy of highway traffic. A) The Fermi level is above the K point in the conduction band. There are many states to occupy. B) The Fermi level is just at the K point. All states in valence band are full. C) The Fermi level is under the K point in the valence band. There are few states to be occupied and these holes moves through the material [121].

Also, if the valence and conducting bands overlaps (as in most of metals), there are many open spaces all the time where electrons can move, so this kind of material are conductors, too. Also,

if the bandgap is relatively small and the Fermi level is between both levels, the material is semiconductor. This means that there are states above the Fermi level which can be occupied, switching thee material from insulating to conducting phase. If the bandgap is so large that the Fermi level often goes from the valence to the conducting band, assuming no charge-carrying electrons removed, this material is an insulator (see Figure 3).

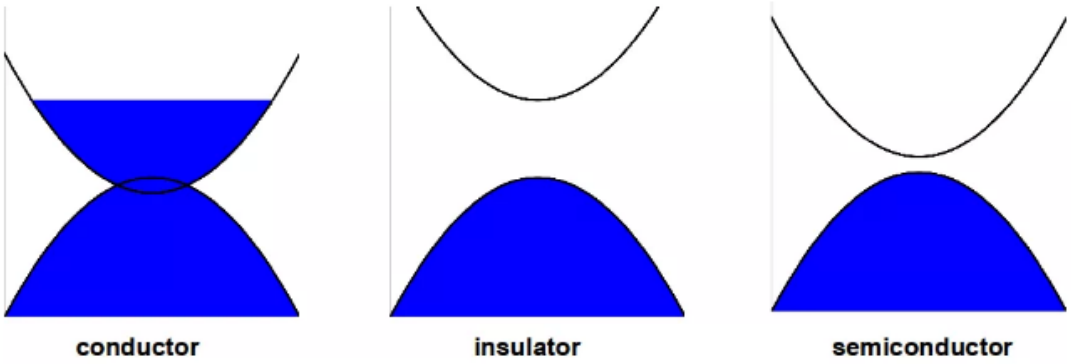

Figure 3. Band level system in different kind of material [121].

2.2. Saturable Absorption

The complicated process and behaviour of saturable absorption can be described as a two-level system. It is considered two levels (E_0 and E_1) with a gap between them of ΔE and infinite possible states for electrons in each level. But it is not taken in account the different electron momentums, just the kind of levels. In other words, there are two levels at two different specific energies, the lowest one (E_0) is at the valence band and the highest (E_1) is at the conduction band, and they have a separation of ΔE.

Considering the system starts with the Fermi level at E_0, if a photon with an energy of ΔE (which is related with Planck's constant and wavelength as $E = \frac{hc}{\lambda}$) hits the system, this photon can be absorbed with a certain probability. This phenomenon can cause that an electron can leave ground its state from E_0 to E_1 level. The photon momentum is added to this electron, but since it is negligible compared to the electron momentum, it can be assumed that the electron momentum will be the same. Therefore, the electron will occupy the analogous position in a higher level with E_1 energy. This phenomenon is called absorption. If the photon energy is the same or larger as the bandgap energy (ΔE), there is a probability of the absorption phenomenon to happen and it is higher as more electrons are in the valence band. However, if the photon energy does not match to bandgap energy, absorption is impossible to occur.

If considering the Fermi level is at the conduction band level, all the electrons will start in the conduction band (see Figure 4.A). Although this consideration is just to model the saturable absorption effect, it must be said that it is physically impossible. There are usually many more electrons in the valence band and this state will be thermodynamically unstable, the electron will fell to E_0 due to different processes such as fluorescence or electron-electron scattering. In this case, if a photon with ΔE energy hits the material, there is some probability that this photon causes an electron fell to ground level with a negligible momentum change, provoking in turn an emission of a second photon with exactly the same energy and momentum as the first one [53]. This process is known as stimulated emission (see Figure 4.B) and it is only possible when an electron is in the conduction band, and is more likely to occur as more electron are in this conduction band.

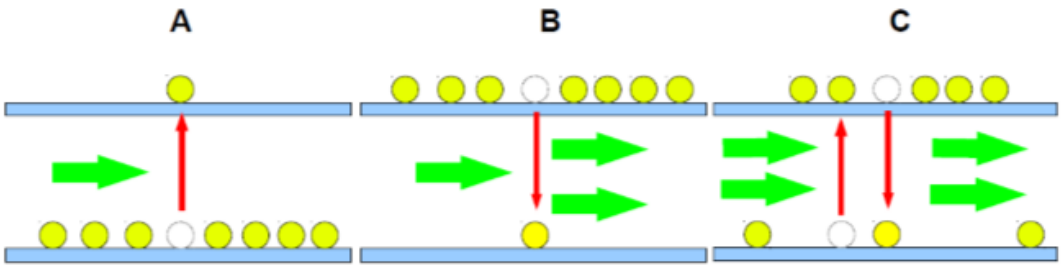

Figure 4. A) Absorption. B) Stimulated emission. C) Saturable absorption. [53]

But it is possible to reach a stable state between absorption and stimulated emission, where the same number of electrons are reached in both band levels. It is achieved when the rate of excited electrons due to absorption equal the amount of electrons that fell from E_1 to E_0 because of stimulated emission and some other process such as electron-electron and electron-photon scattering (see Figure 4.C). This steady-state is named as saturable absorption and is the main cause of the higher order terms of the intensity absorption. This state depends on some inherit properties of the material and band level system, such as the tame it takes to an electron to decay from conduction band to ground level without stimulated emission, the relaxation time of the absorber (time takes the probability of stimulated emission in to decrease to zero) or saturation energy (energy or number of photons needed to decrease the probability of absorption to 1/e).

For saturable absorbers, the pulse duration is much longer than the relaxation time of the absorber, so it makes sense that some percentage of the incident light is instantaneously absorbed by the saturable absorber. Therefore, according to the equations development in [53] a similar equation to Eq. 3 is given, but instead of in space, in time.

2.3. Graphene Band System

As it has been previously mentioned, graphene is a 2D carbon crystal that forms a honeycomb lattice. But there are two sub-lattices according to carbon atom bond orientations (see Figure 6.A). In graphene, the atoms are sp2 hybridized, which means that all atoms of the same layer are linked each other by three covalent σ-bonds (see Figure 5), which are known as the strongest chemical bond ever seen and is the cause of its enormous mechanical material strength [17]. The different layers are linked by π-bounds, which are less strong than the other ones. Moreover, most of graphene singular properties are due to its band structure, and thus that ones that are useful to implement a saturable absorber too.

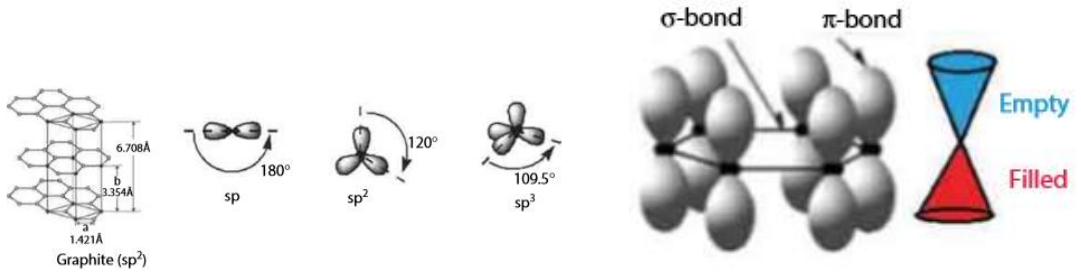

Figure 5. Various hybridizations of carbon and schematic of the in-plane σ bonds and the π orbitals perpendicular to the plane of the graphene sheets [17].

The band structure of graphene was first studied by Phillip Russel Wallace in 1947 and later studied by Neto et al. They deduced that the energy required to a photon to hop from one atom to another atom in next lattice atom is about 2.8 eV. But the energy required to an electron to hop from one atom to another in the same lattice is approximately 0.1 eV. Figure 6.B shows the graphene band structure around the Brillouin zone. As it is shown in this figure, unlike most materials, graphene has some points (actually six) where conducting and valence band touches each other all at the same energy without overlapping. The energy where the bands meet is called the Dirac point and these point are called K points. Therefore, graphene has no bandgap at the K points and for that reason is widely called as “zero bandgap semiconductor”. This property has the consequence that any photon that hit the material, no matter what energy it has, has a probability to be absorbed. This means that graphene’s response is broadly flat in terms of wavelength.

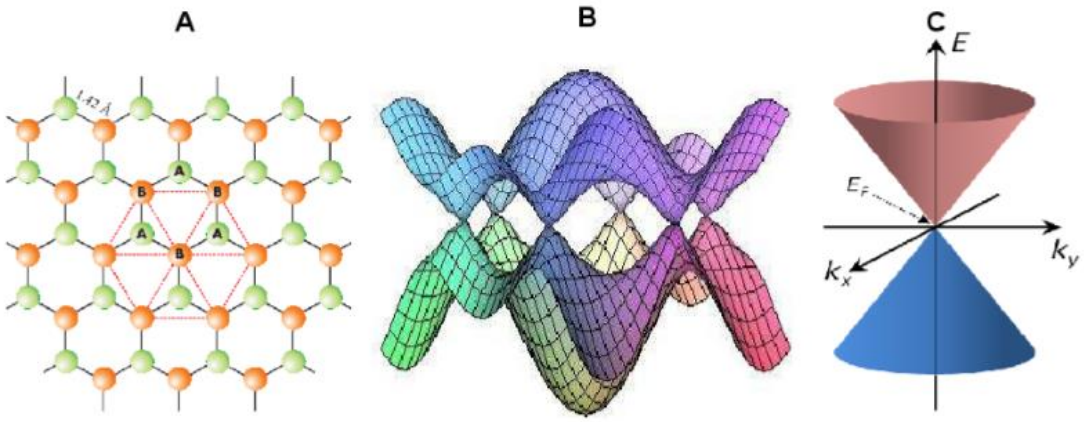

Figure 6. A) Graphene's honeycomb lattice and sub-lattices. B) Graphene band structure. C) Graphene band structure near the Dirac point.

The band structure of graphene can be linearly approximated near the Dirac point, where $v_f \approx 1 \cdot 10^6 m/s$ is the Fermi velocity (velocity at which electrons can travel through the material). One singular property of graphene is that Fermi velocity does not depend on energy or momentum of the electron. The Fermi velocity depends linearly on momentum, which in turn depends on the electron energy. This means that for any energy below approximately 4 eV, electrons have a massless behaviour such as photons, which have a fixed speed [53]. This property makes graphene to have an extremely high conductivity and this linear behaviour also makes graphene to have a 2.3% linear absorption for energies below 4 eV [53]. This absorption is also proportional to the number of layers. Also, as the space between conducting and valence band and the density of states scale linearly with momentum, the absorption probability is the same for a broad range of photon energies. The band structure of graphene near the K points is shown in Figure 6.C. Near the Dirac point it looks like both cones that touches each other at one point. It is because, as it is above mentioned, the energy of charge-carrier scales linearly with the absolute value of momentum.

2.4. Graphene Saturable Absorption

First, it is assumed that graphene starts in an insulating phase because, as two particles cannot be in the same place and all places at conduction band are full (see Figure 7.a), any electron could be excited from valence band to any empty place in conduction band by any photon. Also, as the stimulated emission generates another photon with the same characteristics, it is only possible if there is an empty place in valence band. When an incident photon excites an electron from the valence band to the conduction band (see figure 7.b), that electron losses lots of its energy due to electron (at femtosecond scale) and lattice (at picoseconds scale) scattering (see

Figure 7.c). Thus, this electron will not decay back to the valence band and will make space to more electrons be excited into the conduction band at the same energy. Furthermore, for high enough peak intensities and pulse rates, so many electrons have been excited into the valence band that there are no open spaces in the lower energy conduction band, avoiding absorption or stimulating emission. This means that saturable absorption has been reached.

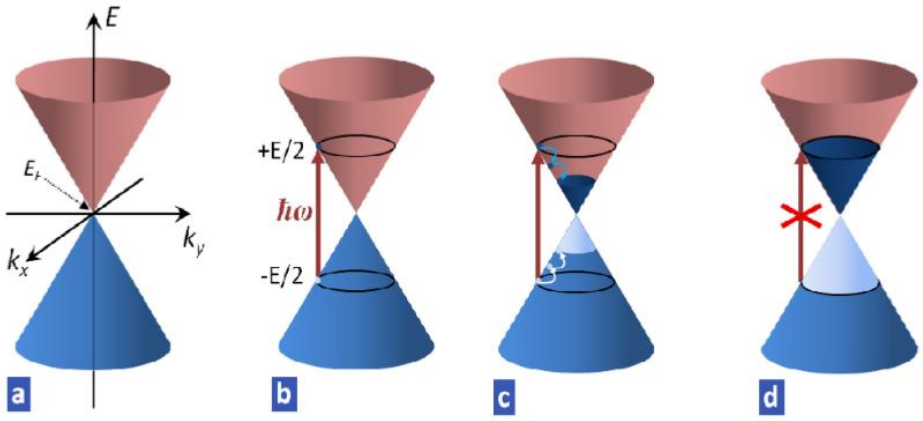

Figure 7. Saturable absorption process in graphene.

Due to the two timescales for electrons relaxation times named above the relaxation time for graphene as a saturable absorber has two components The fastest one is caused by electron-electron scattering and it is in the order of 7 fs [53], so it can be approximated as a fast saturable absorber. The slowest component is mostly caused by electrons falling into the spaces they left in the valence band by dropping into the valence band through the K point. This component can be approximated as a slow saturable absorber, but for simplicity graphene is considered a fast saturable absorber.

2.5. Graphene Doping

One of the greatest advantage of SESAM saturable absorber is its optical properties tunability during production., such as linear absorption, relaxation time or saturable loss. Thus, to compete with SESAMs graphene must have these properties tunability too. On way to achieve this properties tunability is modifying the Fermi level of graphene. It is possible to block absorption shifting graphene either to an electron or hole conduction phase. If graphene is shifted to electron conduction phase, no electrons can be excited from the valence to conduction band because there are not open states at required energy in the conduction band for electrons to be excited. On the other hand, if graphene is shifted to hole conduction phase, neither any electron can be excited from valence to conduction band, but this time because there are no electrons

in the valence band at the required energy to be excited. This state is named as “state blocking” [53].

For semiconductor, in order to modify Fermi level, it is needed to immobilize charges in the material removing carriers from band structure. This immobilization can be done adding some stationary charges to the material and thus, attract these carriers and removing them from the bands system. This method is called “doping”. Figure 8 shows how H+ ions contact the material and attract electrons to the surface forming dipoles between each other. In that way, the number of charge carriers (electrons) are removed from the bad system and thus, the Fermi level decreases and the material becomes hole-doping (or p-doping). In case of holes were immobilized a similar process will be taken, but in this case the material will become electron-doping (or n-doping). For graphene an analogous process occurs, but due to its two dimensional structure it is much more complicated to illustrate.

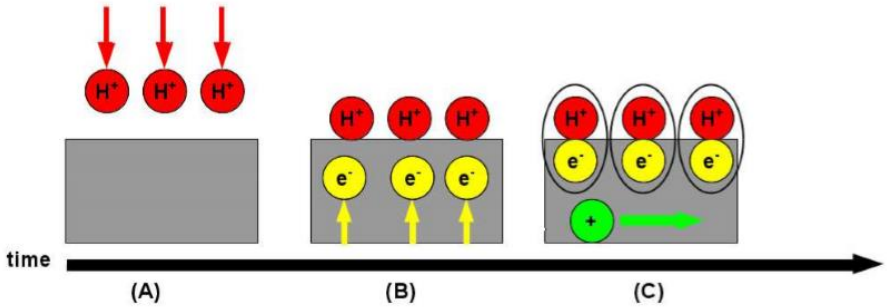

Figure 8. Hole doping of a bulk semiconductor [53].

Less electrons in the valence band means lower probability for an electron to be excited to conduction band and therefore the absorption also decreases. In other words, as the Fermi level shifts away from the K point the absorption decreases continuously, even if the full state block state is not reached. This means the optical absorption can be continuously tuned. Furthermore, as state blocking only affect to photons with twice energy the difference between K point and Fermi level, doped graphene has no constant linear absorption and, in this way, Fermi level can be determined by the absorption spectrum.

But chemical doping is not the only way to modify the Fermi level, also and electrostatically doping can be done. To achieve that, graphene can be placed between an electrode and a dielectric material in a capacitor. Then, when a voltage is applied, the dielectric material polarizes and a charge density is carried out, which behaves as the H+ ions in chemical doping. This charge density attracts and immobilize graphene charges, achieving its doping.

In neutral graphene, the Fermi level is just at the charge neutrality point, that mean that the valence band is fully occupied and the conduction band is empty, but it only occurs at T=0°K. At room temperature, an intrinsic doping makes the Femi level to be placed either somewhere in the valence or in the conduction band. This intrinsic doping can be caused by many factors, such as the presence of several thermal excited carriers at band edge, graphene absorption on a metal substrate or even when a gate bias is applied [123]. Figure 9 shows the band structure for the three different regimes.

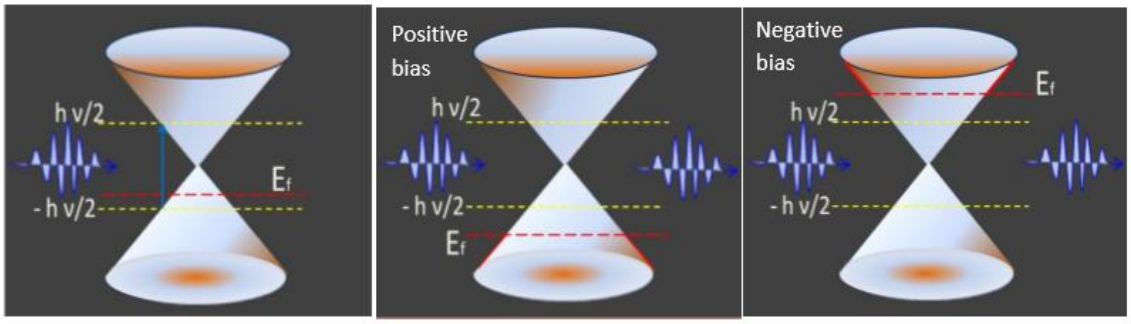

Figure 9. a) Under zero bias condition an incoming photon can be absorbed. b) For positive bias satisfying the transition threshold condition carriers cannot be switched. c) For enough negative bias, there is no open space in the conduction band to an electron be excited [124].

3. Chip Structure

For the graphene characterization, the graphene is patterned as a set of waveguides, which allows a significant light-matter interaction due to the coupling between the evanescent tail of the highly confined waveguide mode and the graphene over a relatively long length. Moreover, this implementation also allows us to control the length and thus the interaction strength.

The silicon nitride design is basically a set of straight waveguides of different widths and lengths. One (at right side) is formed by long waveguides with wides from 1200 nm up to 2400 nm in steps of 200 nm in sets of each 10 waveguides. The other (at left hand side) is formed by two arrays of short waveguides which wides are from 1200 nm up to 2500 nm in steps of 100 nm and also forming groups of 10 waveguides with the same width. Added to this design we transferred and patterned different lengths of graphene, but only one out of two waveguides. The length of the deposited graphene goes from 50 µm to 1600 µm. For the first chips these lengths were [100, 200, 400, 800, 1600] µm for long waveguides and [25, 50, 100, 200, 400] µm for short ones. For later chips, the graphene lengths for long ones were changed to [50, 100, 200, 400, 800] µm because 1600 µm of graphene introduced so much losses that measurements were under the power meter detection level.

The length of these waveguides are 500 µm for short ones and 2185 µm for long ones, added to a pair of tapers of 400 µm. Moreover, to couple the light, a pair of grating coupler are added to each waveguide. However, later chips will be cleaved close to these grating couplers in order reduce coupling losses. Therefore, light will be coupled horizontally using lensed fibers. This will only be done for the large waveguides.

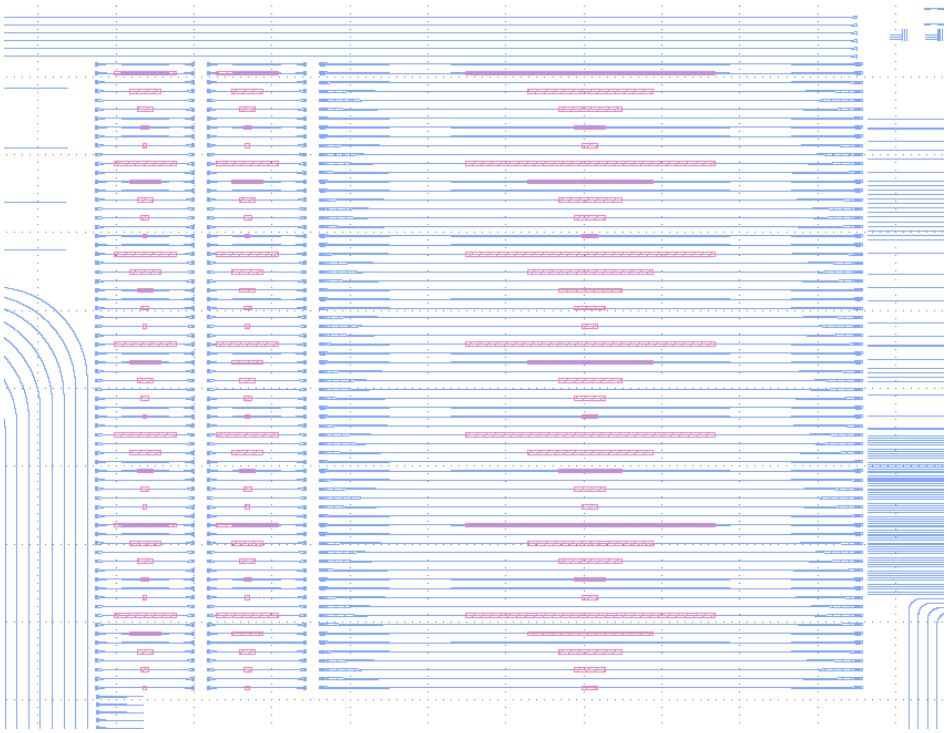

Figure 10. Overall view of waveguides and graphene pattern.

The cross-section is similar to the one in Ref. [117]. Basically, a set of strip LPCVD SiN waveguides of 330 nm thickness is patterned on a top of 3 µm buried oxide layer on a silicon handle wafer (this process is made in a CMOS pilot line). Then the sample is covered with a LPCVD oxide layer of 1 µm that is later thinned down by a combination of chemical polishing, Reactive Ion Etching and wet etching, but a residual oxide layer of about 35 nm thick is remaining. The strip structure also has a residual layer of SiN of about 30 nm, too. After that, a single layer of graphene is grown by Chemical Vapour Deposition (CVP) by an external Spanish company called Graphenea [118] and transferred to the chip, then the previously mentioned graphene patterning is achieved by photolithography and oxygen plasma etching so that different waveguides were covered with different lengths of graphene.

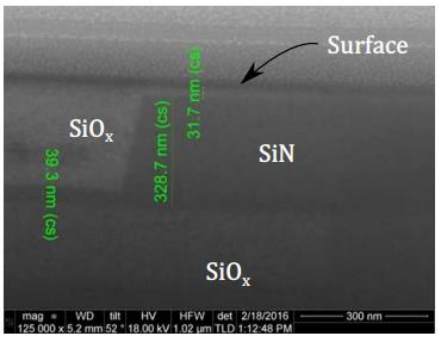

(a) SEM image of the cross-section of a SiN waveguide.

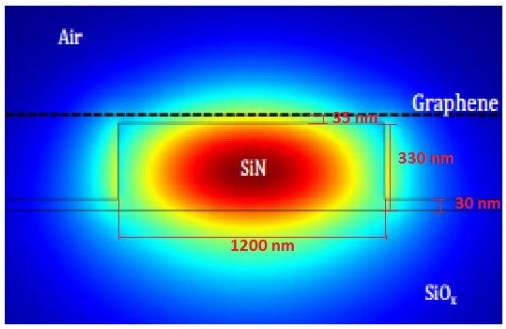

(b) TE mode profile (amplitude of the E-field, COMSOL Multiphysics®). The waveguide width is 1200 nm, the wavelength λ = 1550 nm.

Figure 11: (a) Cross-section of a waveguides and (b) the simulated first order TE mode.

To dope the graphene (or change the Fermi level) and modify its saturable absorption by an electrical voltage, a set of titanium-gold (Ti/Au; ≈ 5 nm/300 nm) metallic contacts are deposited by lift-off with the pattern show in Figure 12. In order to no affect characterization measurements because of sample manipulating or any possible effect of this metallic contacts, the titanium-gold pattern will be deposited after the characterization of coupling losses and graphene saturable absorption without any applied voltage.

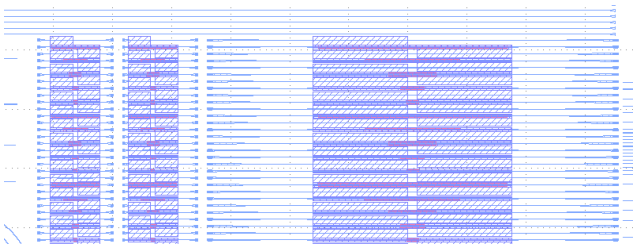

a) Overall view of contact pattern.

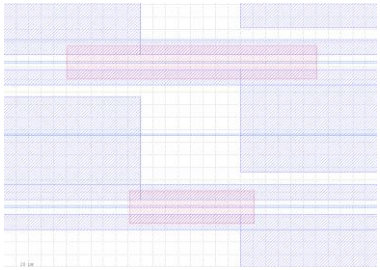

b) Zoom to area of interest.

Figure 12. Image of contact electrodes pattern.

Finally, all the structure is covered with a polymer electrolyte consisting of $LiClO_4$ and polyethylene oxide (PEO) in proportion of 0.1 to 1, each other. This allows to electrostatically change carrier density, and thus, the Fermi level of graphene. Figure 13 shows the cross section of the final sample and gating scheme. In that scheme it appears a little resistance in graphene when applying a certain V_{DS} voltage.

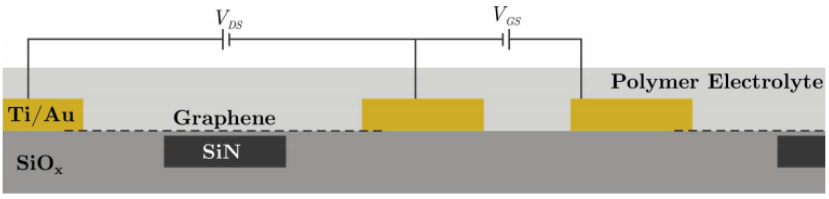

Figure 13. Sample cross section and gating scheme [112].

When applying a gate voltage V_{GS} the carrier density of the graphene can be tuned. According to [122], the dependence of Fermi energy E_F on the gate voltage V_{GS} is approximately:

$$V_{GS} - V_{DS} = sgn(E_F)\frac{e\,E_F^2}{\hbar^2\,v_F^2\,\pi\,C_{EDL}} + \frac{E_F}{e} \qquad (1)$$

With e as the electron charge, $v_f \approx 10^6\ m/s$ the Fermi velocity and C_{EDL} the electric double layer capacitance. V_D the Dirac point, the voltage at which graphene becomes intrinsic and at which the conductance reaches the minimum. This Eq. 1 is derived at T=0K, but at room temperature, the difference is negligible.

4. Linear Loss Characterization

4.1. Setup and Modelling

The first step is the characterization of the chip, specifically graphene losses per unit of length and coupling losses. To get these parameters we must measure the transmission for each wavelength and for different graphene lengths, and the chosen setup is shown in Figure 14.

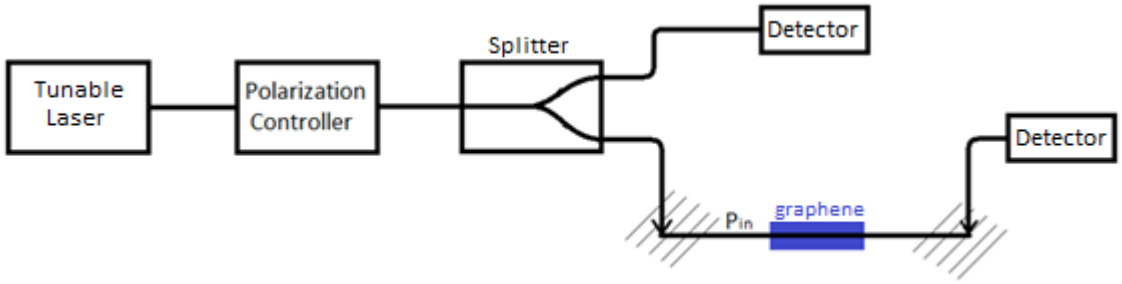

Figure 14. Linear loss measurements setup.

In that way, with Eq. 2 and Eq. 3 it is possible to get the desired data. Moreover, it will be done with the help of a frequency sweep with a continuous tunable laser to get the values in a wide range of wavelengths and show a more complete behaviour (see code in Annex I).

$$P_{in} = 10 \cdot \log_{10}\left(\frac{T_{ref}}{T_{main}}\right) + P_{ref} - L_g \quad (2)$$

$$\text{T [dB]} = \left(P_D + L_g\right) - P_{in} \quad (3)$$

In Eq 1. the input power of the graphene waveguide P_{in} is calculated as the relation in decibels between the output power in both arms of the splitter, added to the detected power in reference detector (P_{ref}) and the losses caused by the grating coupler (L_g). On the other hand, the transmission of the graphene waveguide (understood as the relation between input and put power) is calculated as the difference between the previous input power and the power detected after the waveguide (P_D), added to grating coupler losses.

Then we can process the measured data (see Annex II). The most interesting graph represent the measured losses versus the graphene length, for each wavelength. From this graph we can deduce the graphene losses per unit of length fitting the points with the simple equation $y = \alpha \cdot x + L_c$,where L_c is the coupling losses and |α| is the graphene losses per length unit. But can also plot the coupling losses (n) for all wavelengths and obtain the response of grating couplers, which should have a maximum at designed and desired wavelength. Another graph could plot graphene losses (α) for each wavelength, as previous. This last plot should be flat, as graphene has a flat response for a wide range of frequencies, and from simulations we know we should get a value between 0,01 and 0,1 dB/cm.

4.2. Linear Loss Measurements

The first step is the characterization of the linear loss of the graphene-covered waveguides: the coupling losses and graphene attenuation. As we can see in Figure 15.a, for telecom wavelength of 1550.0 nm and for waveguides with a width of 1800 nm the graphene loss is 0.0403 dB/µm, which is an expected value by simulation. Furthermore, Figure 15.b shows the graphene losses for different wavelengths, which is flat, as it was expected because of the flat response of graphene. For different widths, the shape is almost the same, but for different chips, graphene or coupling coupler losses can differ, due to differences in the fabrication process. To check if the coupling coupler losses are correct, it is possible to measure the losses in some waveguides without graphene and assuming negligible losses inside the waveguide. It must also be mentioned that this graphs have been done in butt coupling setup.

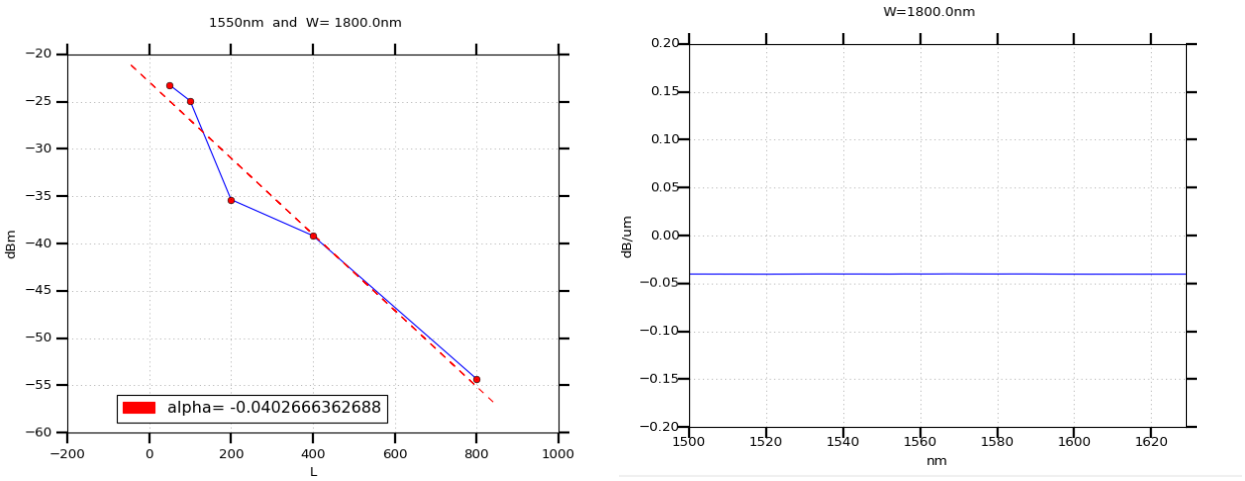

a) Total insertion loss at 1550 nm. b) Graphene losses vs. wavelength.

Figure 15. Waveguides characterization in butt coupling setup for 1800 nm width waveguides.

In case of butt coupling, as the wavelength response is flat, the linear characterization is simpler. First, the fiber-to-fiber power without any sample is measured and taken as input power (P_{in}). Then, the transmission is calculated as shown in Eq. 3, with L_g= 0. The code used is shown in Annex I and II.

5. Saturable Absorption Characterization

5.1. Setup and Modelling

To observe the saturable absorption effect we implement a similar setup than for the characterization, but using a variable attenuator and a pulsed laser instead of continuous one (see Figure 16). To observe this effect, a large peak optical power is needed and the simplest way to achieve that is by using a pulsed laser. Also, a continuous wave laser with such high power will burn the deposited graphene.

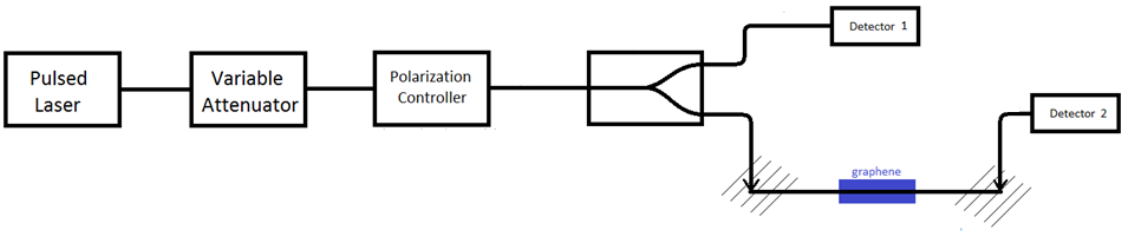

Figure 16. Saturable absorption scheme.

But the use of femtosecond lasers carries some inconveniences since fiber dispersion broadens the pulses and reduces its peak power. For that reason, it is necessary to reduce the fiber lengths as much as possible. One possibility in account is to use a pair of collimators and a variable

wheel-attenuator in order to avoid the fiber length of a typical variable misalignment-attenuator. Moreover, fiber lengths in the splitter, polarization controller and fiber sections has been shortened by making fusion splices if necessary. Therefore, the resulting setup looks like in Figure 17.

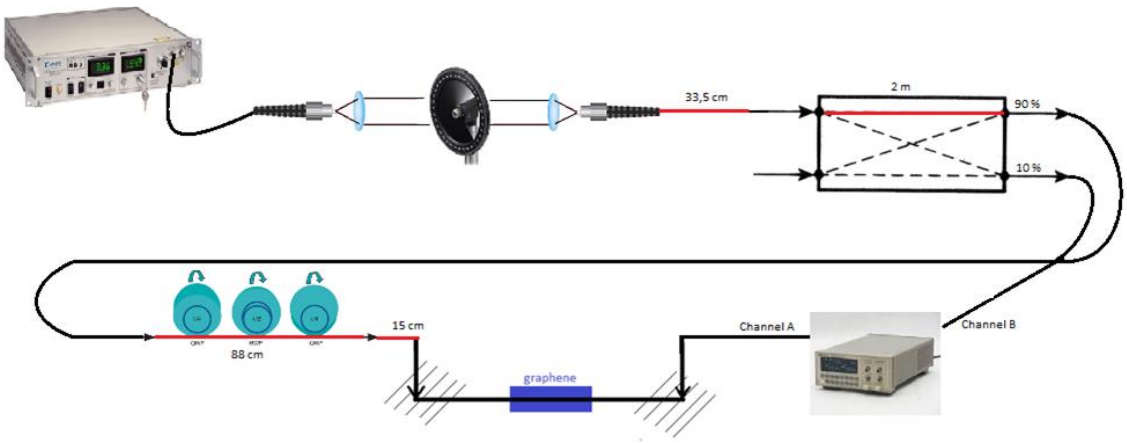

Figure 17. Real implemented setup.

To ensure that the peak power coupled into the waveguide is sufficient to observe the saturable absorption, a previous simulation of pulse propagation along this set up is carried out. For that, a Matlab code provided by Photonics Research Group of Ghent University is used.

As for the shortest Calmar laser pulse widths the matlab code is not accurate, a 100 mA of pump current in pulsed laser is taken. The simulated values are shown in Table 1 and each step of simulation is shown in Figure 18.

Point	0	1	2	3	4	5	6
P_peak [W]	1630	1375	434.8	112.4	53.80	52.71	3.33
P_peak [dBm]	62.12	61.38	56.38	50.51	47.31	47.22	35.22
FWHM [ps]	0.197	0.2243	0.2243	0.8208	0.8208	0.5863	0.5863
τ [ps]	0.12725	0.12725	0.12725	0.46565	0.46565	0.33261	0.33261
P_avg [mW]	7.30	7.01	2.22	2.10	1.00	0.70	0.056
P_avg [dBm]	8.63	8.46	3.46	3.22	0.02	-1.53	-13.53

Table 1. Simulated values of broadening pulse.

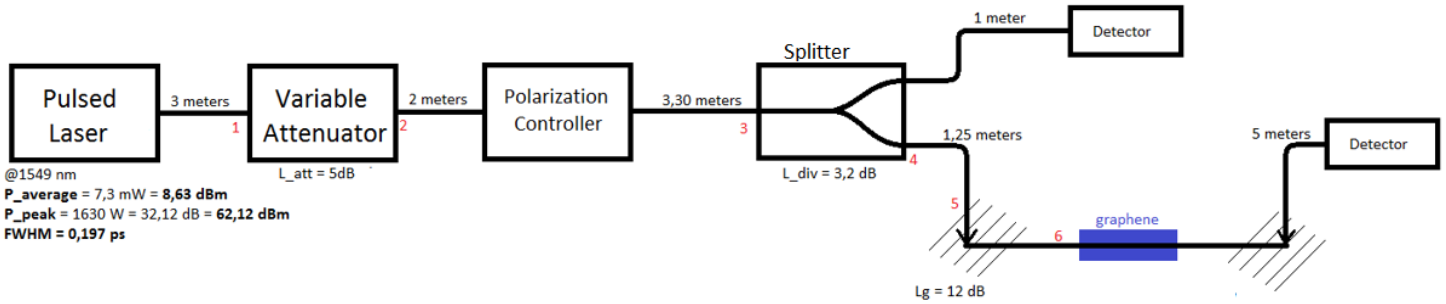

Figure 18. Simulated points for broadening analysis.

This analysis is just to have an idea of the peak power values. Taking [119] as reference, we can assume that a simulated value of 46.10 dBm is enough to observe graphene saturable absorption. In [109] a similar research has been carried out, but employing silicon waveguides, not SiN. Nevertheless, as we can use more input power, to ensure that we will detect saturable absorption, the pumped current used will be 200 mA for all next measurements, taking care of not exposing graphene to this high optical power, in order to not burn the material.

Figure 19 shows how a pulse of 197 femtoseconds width is broaden after 2 meters of standard monomode fiber optic. This pulse width corresponds to an EDFA pumped current of 100 mA (see Table 2) used in the previous simulation.

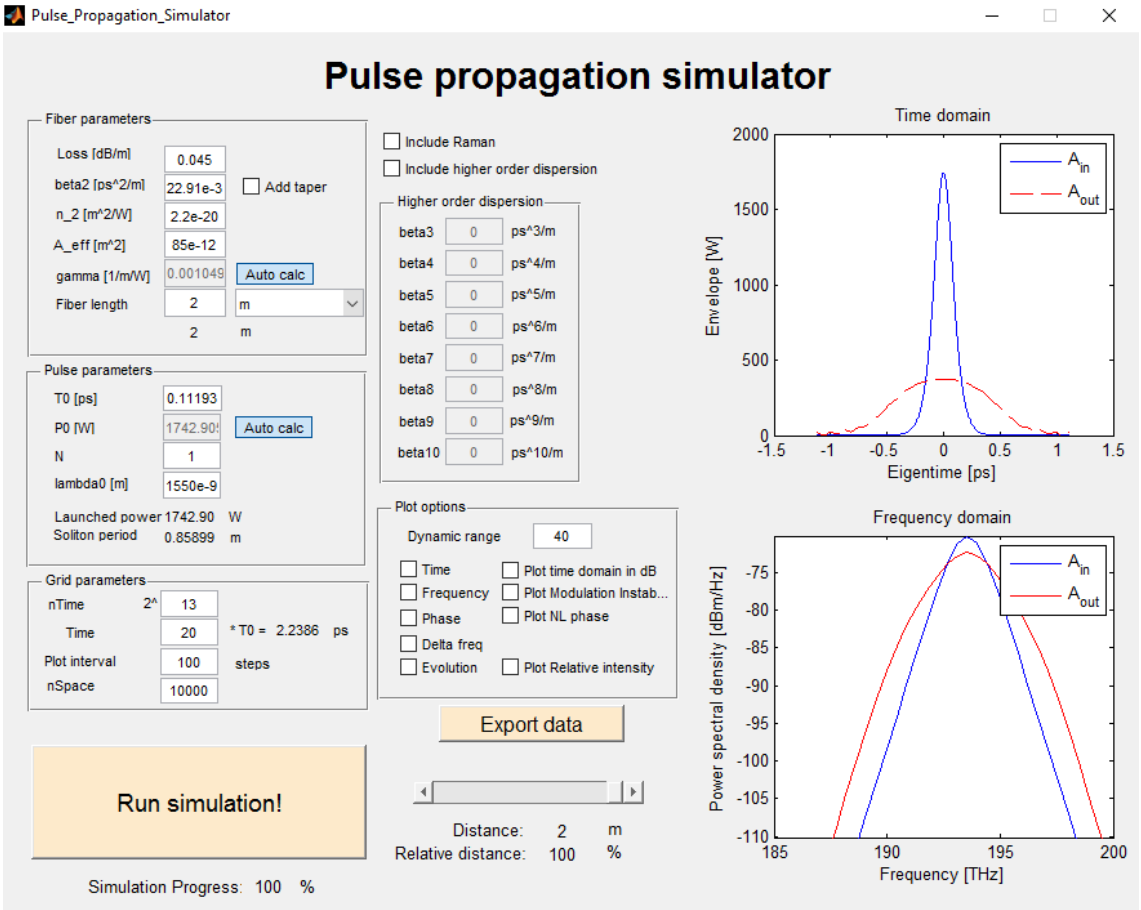

Figure 19. Pulse propagation simulation for 0.045 dB/m losses, $\beta_2 = 22.91 \cdot 10^{-3} Ps^2/m$, $n_2 = 2.2 \cdot 10^{-20} m^2/W$, $A_{eff} = 85 \cdot 10^{-12} m^2$, λ = 1549 nm, τ = 0.11193 ps, 2 m of fiber length and with Raman effects included. The fiber specifications are taken from Corning SMF-28 fiber.

5.2. Saturable Absorption Measurements

Figure 20 clearly shows the saturable absorption effect. The low power of -6 dBm is expected since the graphene loss is about 6 dB ($100\ \mu m \cdot 0.06\ {}^{dB}/_{\mu m} = 6\ dB$). In that sample has been taken in account an input power about 11.6 dBm and 11.2 dB losses for each grating coupler, added to 5.5 dB losses due to connectors and intermediate devices. The input power inside the waveguide is the average power of the pulse train, not the peak power, as obtaining an exact value of this data would require a full knowledge of each setup device behaviour and a process data for each abscissa point would take too long time without providing much more information.

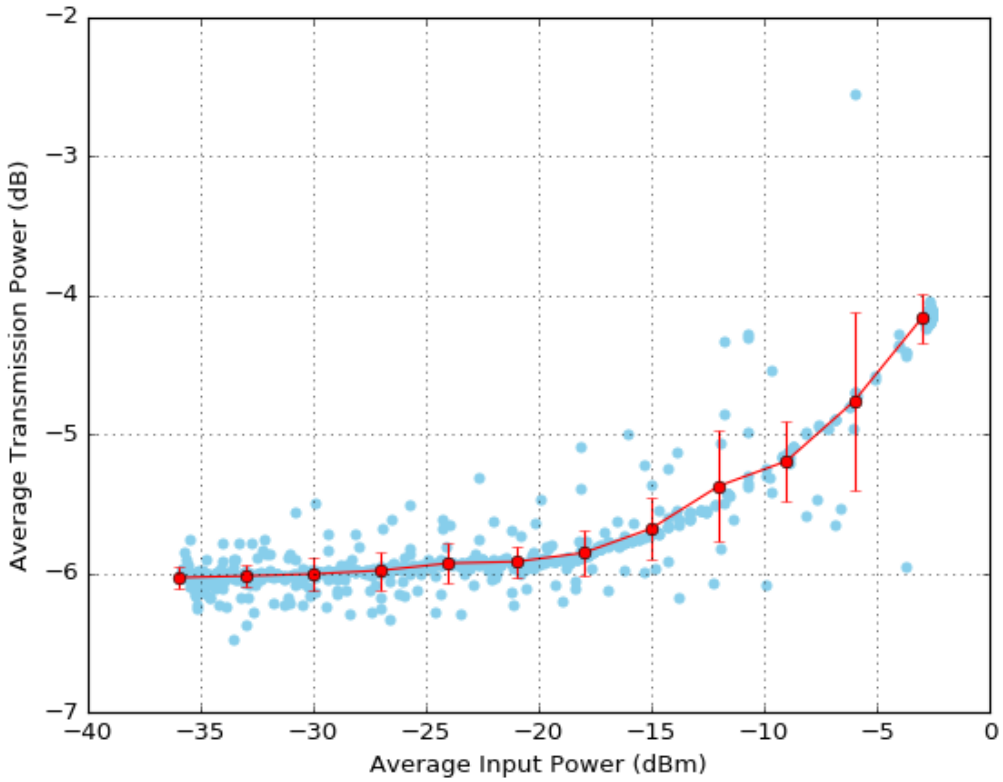

Figure 20. Data from waveguide with 1.9 µm width, 100 µm graphene length and 200 mA of pump current in the pulsed laser. The vertical axis is the transmission (dB) in terms of average input and output power and the horizontal axis is the average input power (dBm).

Theoretically, saturable absorption would increase to achieve full transmission, but getting a power increase of 2 dB, as shown in Figure 20, is still a great result. This effect has been

demonstrated for the rest of waveguides, too. Nevertheless, graph points present so much dispersion because of the measurement system, but it can be reduced averaging in stretches and plotting the typical deviation (see Annex IV).

5.3. Saturable Absorption Tunability

The next step that is carried out is gating the graphene in order to tune the saturable absorption. To observe this result a set of different voltages has been applied to the waveguides, from 0 mV 1200 mV in steps of 100 mV. Also, as it is mentioned in section 2, firstly an ionic gel above graphene is deposited in order to be able to control the saturable absorption.

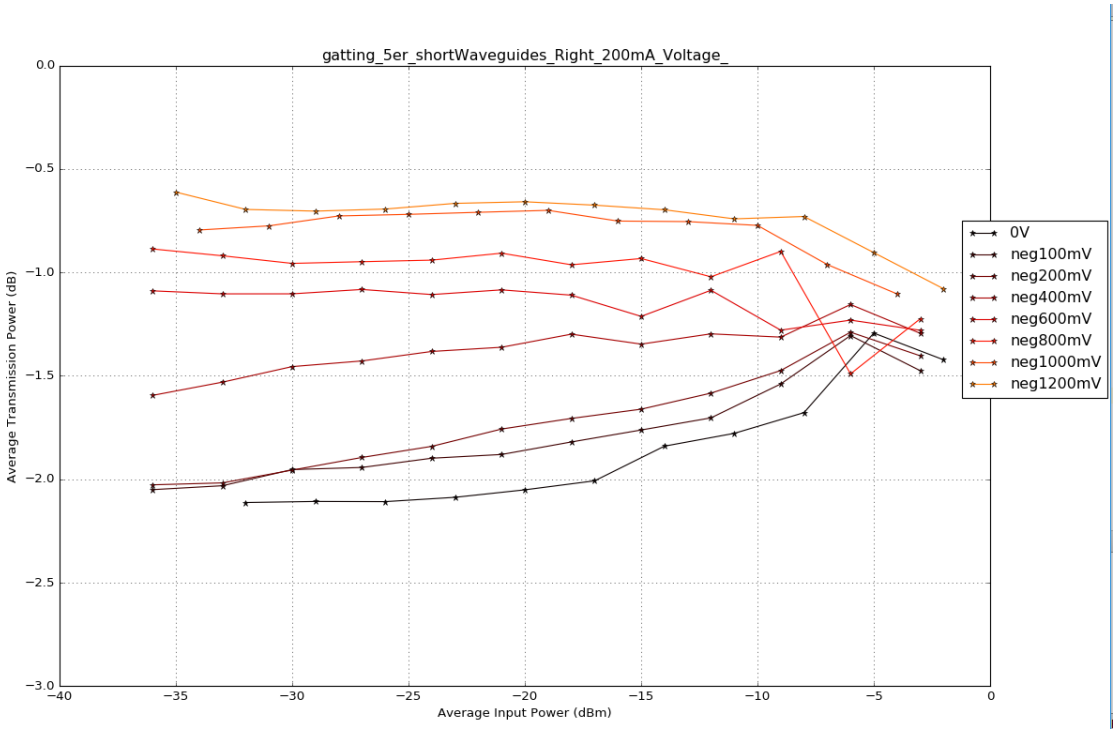

Figure 21. Average input power vs. transmitted power for 1200 nm width waveguide and 100 µm graphene, measured with 200 mA of pump current in pulsed laser and gating voltages from 0V to 1.2 V negative connected.

Figure 21 clearly shows how the graphene saturable absorptions is modified by applying a voltage and thus gating it and shifting its femi-level. As the graphene length is only 100 µm, the change is not as intense as for longer lengths, as it is seen comparing with Figure 22. It must be mentioned that the total absorption has been normalized, estimating grating coupling losses and it can be slightly different, moving all the plotted data up or down.

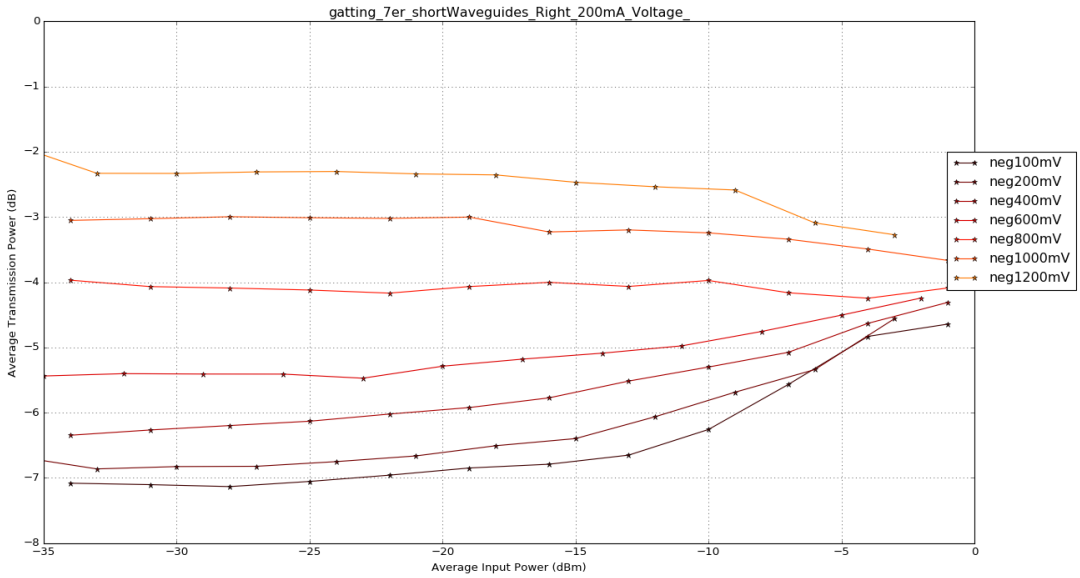

Figure 22. Average input power vs. transmitted power for 1200 nm width waveguide and 200 µm graphene, measured with 200 mA of pump current in pulsed laser and gating voltages from 0V to 1,2 V negative connected.

As it is seen in Figure 21 and 22, for high doping and high input power, the graphene does not behave as a saturable absorber. According to [126], the reason is that multiphoton process come into play.

To simulate how the absorption is modified by the voltage and to be able to fit a suitable shape to these graphs, the phenomenological model in Eq. 4 is used [120]. This equation shows how the attenuation α depends on power (P) at any position. Therefore, the main parameters that must been deduced to characterize that tunability are α_0 (the low-power limit of the attenuation) and P_0 (the saturation power limit).

$$\alpha(P) = \frac{\alpha_0}{1+\frac{P(z)}{P_0}} \qquad (4)$$

In order to deduce these two parameters, an integral equation (Eq. 5) must be solved, where $P|_w = abs(A|_V)^2$. To get it deduced it is necessary to integrate as seen in Figure 23.

$$\frac{\partial A}{\partial z} = -\frac{\alpha(P)}{2} \cdot A \qquad (5)$$

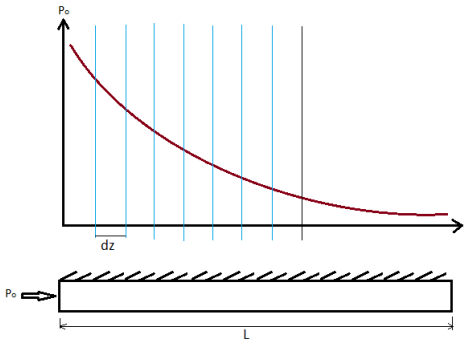

Figure 23. Scheme of input power dependant losses integral equation for a waveguide.

If we integrate Eq. 5 numerically as shown in Figure 23 we can approximate it by obtain Eq. 6 and therefore it will be possible to obtain the output power as function of input power, graphene length and parameters α_0 and P_0, where $\alpha|_{dBm/m} = \alpha|_{1/m} \cdot 10 \cdot log10(e)$ and $\alpha(P) = \frac{\alpha(A)}{2}$. It is also known that $T = \frac{P_{out}|_W}{P_{in}|_W}$, which is proportional to $\frac{1}{\alpha}$. It is implemented in a Python code as shown in Annex V.

$$A(z+dz)|_V \approx A(z)|_V - \frac{\alpha[A(z)]|_{1/\mu m}}{2} \cdot A(z)|_V \cdot \Delta z|_{\mu m} \qquad (6)$$

However, in order to achieve higher on-chip powers and go further obtaining better graphs, it is interesting to avoid grating couplers, which introduce high insertion losses. For that reason, the chip is cleaved next to these grating couplers for the longer waveguides. However, there can be a mismatch between the field profile coupled into the waveguide and the field of the waveguide mode. Hence, this overlap is simulated for different waveguide widths in Lumerical software. The used code can be seen in Annex VI.

As it is shown in Figure 24, the overlap losses are about 3.5 dB, which is much lower than calculated values for grating couplers.

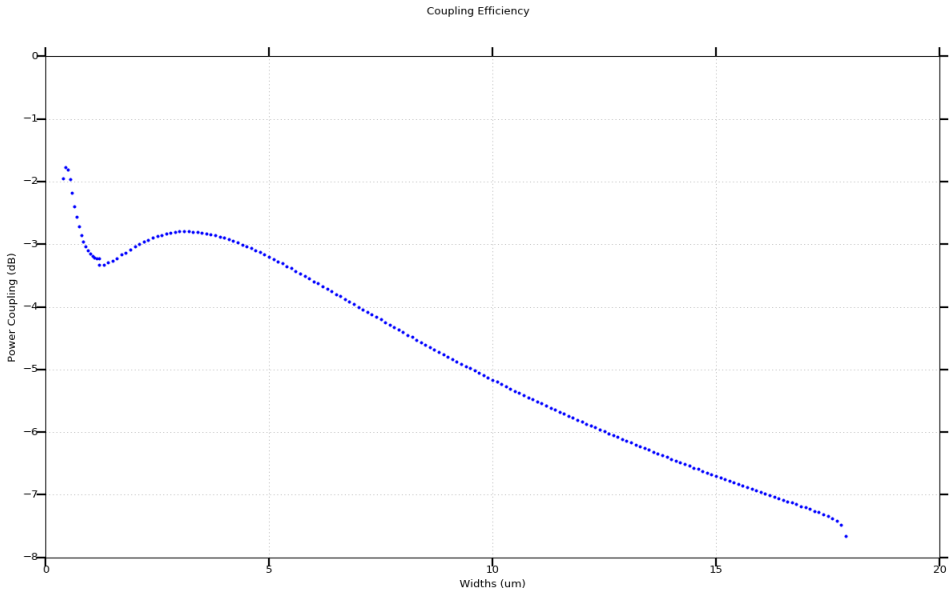

Figure 24. Overlap between waveguide and coupling field simulated with Lumerical software.

6. Technical specification

6.1. Detector

The detector used for all setups is the model Hewlett Packard (HP) 8153A, with which two equal power sensors have been used. These power sensors are the model HP 815131A, which have a wavelength range from 800 to 1700 nm.

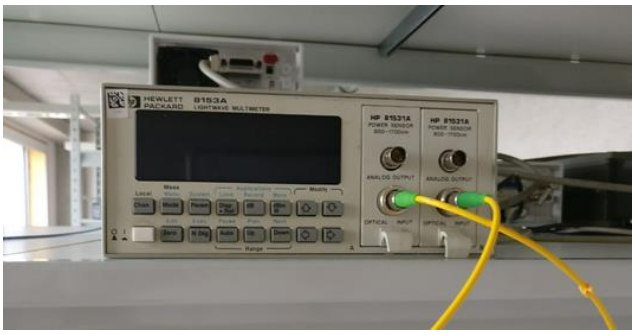

Figure 25. Power meter HP 8153A.

For low input powers we can reach the sensitivity level of the power sensor and the measurements could be affected as an increasing transmitivity for low input powers, as has been seen in some measurements. For that reason, to ensure that this increasing is due to the power meter sensitivity and not to other causes, we implement the same setup, but replacing the SiN-graphene waveguide by another variable attenuator, as we can see in next figure. In that way

we can simulate the waveguide and coupling losses adjusting the variable attenuator and avoid the saturable absorption effect of the waveguides, too.

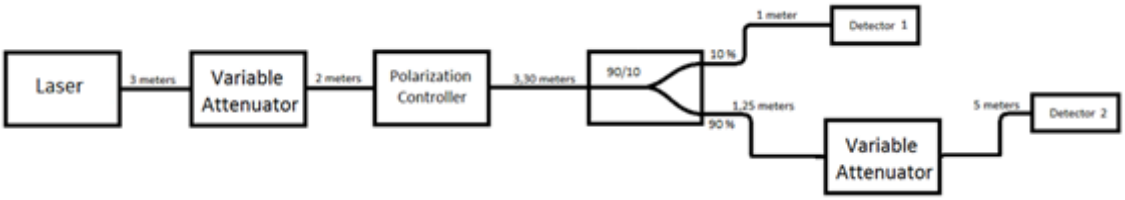

Figure 26. Setup for testing power meter.

First set both variable attenuators to get -35 dBm in Detector 1 and -65 dBm in Detector 2, because these are the values obtaining while measuring a real waveguide. Then, the first variable attenuator is moved in order to get similar measurements, which are plotted in Figure 27.

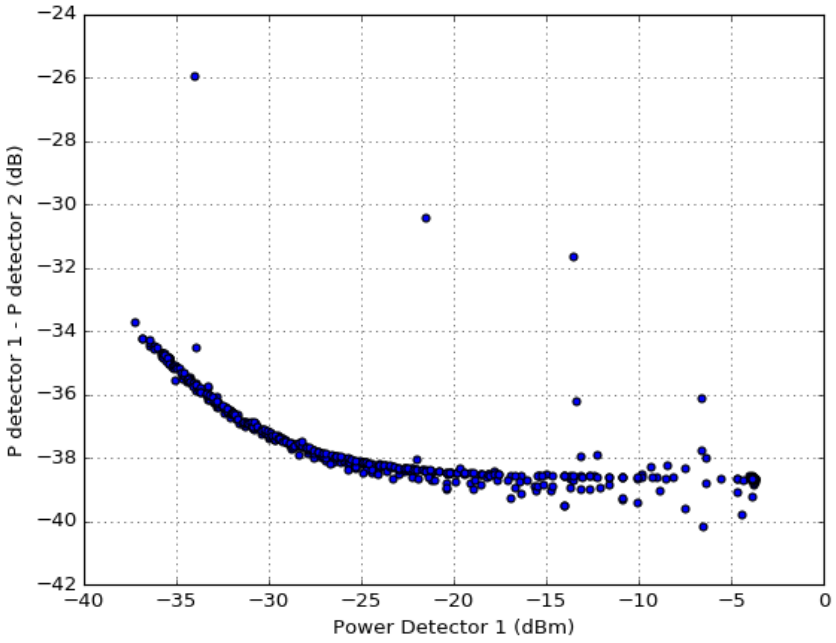

Figure 27. Measurements Power Meter HP 8153A.

To take a value as threshold, it is assumed that measurements from -25 dBm detected in Detector to downwards are not accurate.

6.2. Tunable Continuous-wave Laser

For aligning, characterization of devices, etc. a standard tunable laser has been used. Such as Tunics Laser model T100S-HP, Syntune Laser model S7600 or Santec model TSL-510.

6.3. Pulsed Laser

To see the saturable absorption phenomenon a high peak power is needed. For that reason, a pulsed laser is used for the measurements, instead of using a continuum one. This kind of lasers achieves a train of pulses with a very high power but with very short widths. The femtosecond laser used to plot the graphs in this thesis has been the Calmar Laser model Mendocino. The specifications of this laser can be viewed in Table 2.

Pump Current EDFA (mA)	Wavelength (nm)	Spectrum width (nm)	P_avg (mW)	Pulse width FWHM (ps)	Repetition Rate (MHz)	P_peak (KW)
50	1548.93	9.49	2.8	0.327	20	0.377
100	1548.75	15.49	7.3	0.197	20	1.630
150	1548.77	22.86	11.2	0.119	20	4.141
200	1549.14	30.67	14.6	0.080	20	8.030
239	1549.78	33.69	17.0	0.074	20	10.108

Table 2. Specification Calmar Femtosecond Pulsed Laser.

This table has been taken the data form attached laboratory catalogue and so the shape of the pulses shown in Eq. 7. For $Sech^2$ pulses, the peak power can be written as Eq. 8, where the pulse energy is P_{avg} multiplied by T (repetition rate) for regular trains and negligible power between pulses.

$$P(t) = P_p \cdot \operatorname{sech}^2(t/\tau) = \frac{P_p}{\cosh^2(t/\tau)} \qquad (7)$$

$$P_{peak} \approx 0.88 \cdot \frac{Pulse\ Energy}{FWHM} \qquad (8)$$

6.4. Lensed Fibers

The lensed fibers used to couple the light are from OZ-Optics. These are single mode Tapered fibers, see Figure 28. The main parameter is the beam radius at the focus length, which is 2.5 µm.

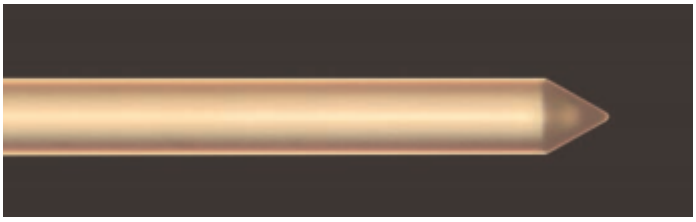

Figure 28. Lensed Fiber from OZ-Optics.

6.5. Splitter

The splitter used in the setups is a fiber based 90/10 divisor. It simply splits the power in both sides at different proportion. In order to avoid pulse broadening due to dispersion as much as possible, the fiber lengths have been shortened as much as possible, using fusion to splice them.

Figure 29. Divisor used in setups.

7. Conclusion and Future Works

7.1. Conclusion

In conclusion, saturable absorption in graphene-covered silicon nitride waveguides has been demonstrated in this thesis. For achieve this result, a series of setups have been implemented in order to improve the graphs. Since simulations shows that such a short pulses broadening can affect the measurements, the fiber lengths in these setups have been reduced as much as possible so that the pulse does not broaden through the fiber due to dispersion effects, and thus reducing the peak power. For that reason, a manually variable attenuator based on a fiber misalignment has been substituted by a couple of collimators between which a wheel attenuator is placed. Also, the fiber length of the splitter, as well as all fiber connections, have been shorten with fusion splices as much as possible. Moreover, as the grating coupling losses were quite high (minimum value got of 8.6 dB per grating coupler), the samples have been cleaved by the long waveguides. Therefore, the vertical measured system was replaced by a horizontal one, based on lensed fibers instead of grating couplers.

After a large set of measurements in a set of samples, where the manually variable attenuation can affect the measurements by appearing a kind of hysteresis, the saturable absorption concept has been demonstrated. As it was expected, the measured graphene losses got are between 0.04 and 0.07 dB/µm. But not only graphene saturable absorption has been tested but

also its electrical tenability. Is has been observed that with a few hundreds of millivolts, a great absorption variation is achieved.

In the chip fabrication, graphene and gold-titanium mask have been designed by IPKISS software run in Python code and then patterned in the samples. Python code has been also used to process all measured data, as well as to plot all the graphs and to remotely control the laboratory equipment.

All these conceptual demonstrations allow the main goal of implement a mode-locked fiber laser and. But the highest interest is, once achieved it, get a possible fully integrated laser which uses graphene for mode-locking and makes profit of its unique properties.

7.2. Future Tasks

Once the saturable absorption phenomenon has been demonstrated, it can be used for a mode locked laser which avoids two photon absorption effect at telecom wavelengths, due to its larger gap. But it would be first needed to improve the results obtained, optimizing the graphene length and waveguide width, as well as a full electrical tunability characterization.

Another possibility is to deduce the drain current in graphene. To achieve that, a set of different electrodes have been implemented in the lithography mask for some waveguides. As the chip has a large set of waveguides, we can dedicate some of them to this purpose, specifically it was carried out for the some of the short ones. Also it has been done to different waveguide widths (see Figure 30).

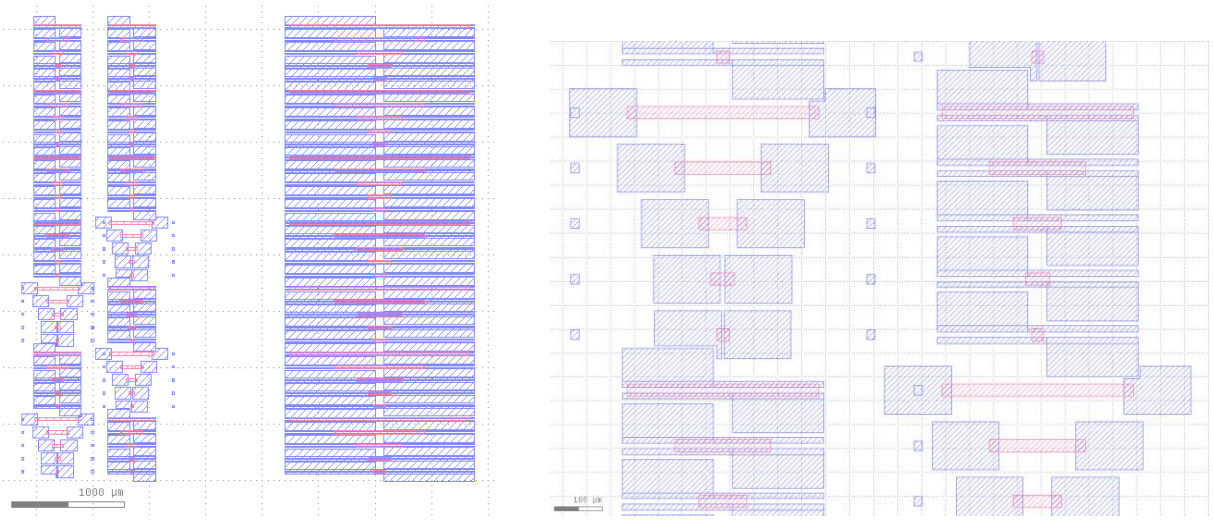

a) Overall view of lito mask. b) Zoom to interest zone.

Figure 30. Set of electrodes for drain current measurements.

Bibliography

[1] T. Kobayashi et al. In Proceedings of the 145th International Conference, pages 13–15. Springer Series in Chemical Physics, 2005.

[2] R. Holzwarth et al. Optical frequency synthesizer for precision spectroscopy. Physics Review Letters, 85:2264–2267, 2000.

[3] D.J. Jones et al. Carrier-envelope phase control of femtosecond mode-locked lasers and direct optical frequency synthesis. Science, 288:365–365, 2000.

[4] K. Minoshima et al. High-accuracy measurement of 240-m distance in an optical tunnel by use of a compact femtosecond laser. Applied Optics, 39:5512–5517, 2000.

[5] T.R. Schibli et al. Displacement metrology with sub-pm resolution in air based on a fs-comb wavelength synthesizer. Optics Express, 14:5984–5993, 2006.

[6] U. Keller. Progress in Optics, volume 46, chapter 1. Ultrafast Solid-State Lasers, pages 1–117. Elsevier, 2004.

[7] I. P. Ippen. Principles of passive mode locking. Applied Physics B, 58:159–170, 1994.

[8] H. A. Haus. Theory of mode locking with a slow saturable absorber. IEEE Journal of Quantum Mechanics, QE-11(9), 1975.

[9] H. A. Haus. Theory of mode locking with a fast saturable absorber. Journal of Applied Physics, 46(7), 1975.

[10] W. Drexler et al. Ultrahigh resolution optical coherence tomography of the human retina. Nature Medicine, 7:502–507, 2001.

[11] M.C. Stowe et al. High resolution atomic coherent control via spectral phase manipulation of an optical frequency comb. Physics Review Letters, 96:153001–153001, 2006.

[12] Z. Zhu et al. Pump-probe spectroscopy of exciton dynamics in (6,5) carbon nanotubes. Physical Chemistry C, 111:3831–3835, 2007.

[13] T. Steinmetz et al. Laser frequency combs for astronomical observations. Science, 321:1335–1337, 2008.

[14] T.R. Schibli. Combs for dark energy. Nature Photonics, 2:712–713, 2008.

[15] C.-H. Li et al. A laser frequency comb that enables radial velocity measurements with a precision of 1 cm/s. Nature, 452:610–612, 2008.

[16] J. Kim et al. Drift-free femtosecond timing synchronization of remote optical and microwave sources. Nature Photonics, 2:733–736, 2008.

[17] Sharon, M. and Sharon, M. (2015) Applications of Graphene, in “Graphene: An Introduction to the Fundamentals and Industrial Applications”, John Wiley & Sons, Inc., Hoboken, NJ, USA. pp. 1-15.

[18] Shank, C. V., & Ippen, E. P. (1974). Subpicosecond kilowatt pulses from a modelocked cw dye laser. Applied Physics Letters, 24(8), 373-375.

[19] Fork, R. L., Greene, B. I., & Shank, C. V. (1981). Generation of optical pulses shorter than 0.1 psec by colliding pulse mode locking. Applied Physics Letters, 38(9), 671-672.

[20] Fermann, M. E., Galvanauskas, A., & Sucha, G. (Eds.). (2002). Ultrafast Lasers: Technology and Applications (Vol. 80). CRC Press.

[21] Mark, J., Liu, L. Y., Hall, K. L., Haus, H. A., & Ippen, E. P. (1989). Femtosecond pulse generation in a laser with a nonlinear external resonator. Optics Letters, 14(1), 48-50.

[22] Ippen, E. P., Haus, H. A., & Liu, L. Y. (1989). Additive pulse mode locking. JOSAB, 6(9), 1736-1745.

[23] Krausz, F., Spielmann, C., Brabec, T., Wintner, E., & Schmidt, A. J. (1990). Selfstarting additive-pulse mode locking of a Nd: glass laser. Optics Letters, 15(19), 1082-1084.

[24] Haus, H. A., Fujimoto, J. G., & Ippen, E. P. (1991). Structures for additive pulse mode locking. JOSA B, 8(10), 2068-2076.

[25] Goodberlet, J., Jacobson, J., Fujimoto, J. G., Schulz, P. A., & Fan, T. Y. (1990). Self-starting additive-pulse mode-locked diode-pumped Nd: YAG laser. Optics Letters, 15(9), 504-506.

[26] Spence, D. E., Kean, P. N., & Sibbett, W. (1991). 60-fsec pulse generation from a self-mode-locked Ti: sapphire laser. Optics Letters, 16(1), 42-44.

[27] Brabec, T., Spielmann, C., Curley, P. F., & Krausz, F. (1992). Kerr lens mode locking. Optics Letters, 17(18), 1292-1294.

[28] Cerullo, G., Silvestri, S. D., & Magni, V. (1994). Self-starting Kerr-lens mode locking of a Ti: sapphire laser. Optics Letters, 19(14), 1040-1042.

[29] Morgner, U., Kärtner, F. X., Cho, S. H., Chen, Y., Haus, H. A., Fujimoto, J. G., Ippen, E. P., Scheuer, V., Angelow, G., & Tschudi, T. (1999). Sub-two-cycle pulses from a Kerr-lens mode-locked Ti: sapphire laser. Optics Letters, 24(6), 411-413.

[30]1 Bouma, B. E., & Fujimoto, J. G. (1996). Compact Kerr-lens mode-locked resonators. Optics Letters, 21(2), 134-136.

[31] Bouma, B. E., Tearney, G. J., Bilinsky, I. P., Golubovic, B., & Fujimoto, J. G. (1996). Self-phase-modulated Kerr-lens mode-locked Cr: forsterite laser source for optical coherence tomogrphy. Optics Letters, 21(22), 1839-1841.

[32] Cho, S. H., Bouma, B. E., Ippen, E. P., & Fujimoto, J. G. (1999). Low-repetitionrate high-peak-power Kerr-lens mode-locked Al2O3 laser with a multiple-pass cavity. Optics Letters, 24(6), 417-419.

[33] Liu, H., Nees, J., & Mourou, G. (2001). Diode-pumped Kerr-lens mode-locked Yb:KY(WO4)2 laser. Optics Letters, 26(21), 1723-1725.

[34] Cho, S. H., Kärtner, F. X., Morgner, U., Ippen, E. P., Fujimoto, J. G., Cunningham, J. E., & Knox, W. H. (2001). Generation of 90-nJ pulses with a 4-MHz repetition rate Kerr-lens mode-locked Ti:Al2O3 laser operating with net positive and negative intracavity dispersion. Optics Letters, 26(8), 560-562.

[35] Durfee, C. G., Storz, T., Garlick, J., Hill, S., Squier, J. A., Kirchner, M., Taft, G., Shea, K., Kapteyn, H., Murnane, M., & Backus, S. (2012). Direct diode-pumped Kerr-lens mode-locked Ti: sapphire laser. Optics Express, 20(13), 13677-13683.

[36] Tolstik, N., Sorokin, E., & Sorokina, I. T. (2013). Kerr-lens mode-locked Cr: ZnS laser. Optics Letters, 38(3), 299-301.

[37] Keller, U., Miller, D. A. B., Boyd, G. D., Chiu, T. H., Ferguson, J. F., & Asom, M. T. (1992). Solid-state low-loss intracavity saturable absorber for Nd: YLF lasers: an antiresonant semiconductor Fabry–Perot saturable absorber. Optics Letters, 17(7), 505-507.

[38] Keller, U., Weingarten, K. J., Kartner, F. X., Kopf, D., Braun, B., Jung, I. D., Fluck, R., Honninger, C., Matuschek, N., & Aus der Au, J. (1996). Semiconductor saturable absorber mirrors (SESAM's) for femtosecond to nanosecond pulse generation in solid-state lasers. Selected Topics in Quantum Electronics, IEEE Journal of, 2(3), 435-453.

[39] Hasan, T., Sun, Z., Wang, F., Bonaccorso, F., Tan, P. H., Rozhin, A. G., & Ferrari, A. C. (2009). Nanotube–polymer composites for ultrafast photonics. Advanced Materials, 21(38-39), 3874-3899.

[40] Adams, L. E., Kintzer, E. S., Ramaswamy, M., Fujimoto, J. G., Keller, U., & Asom, M. T. (1993). Mode locking of a broad-area semiconductor laser with a multiplequantum-well saturable absorber. Optics Letters, 18(22), 1940-1942.

[41] Steinmeyer, G., Sutter, D. H., Gallmann, L., Matuschek, N., & Keller, U. (1999). Frontiers in ultrashort pulse generation: pushing the limits in linear and nonlinear optics. Science, 286(5444), 1507-1512.

[42] Holmgren, S. J., Fragemann, A., Pasiskevicius, V., & Laurell, F. (2006). Active and passive hybrid mode-locking of a Nd:YVO4 laser with a single partially poled KTP crystal. Optics Express, 14(15), 6675-6680.

[43] Lecaplain, C., Chédot, C., Hideur, A., Ortaç, B., & Limpert, J. (2007). High-power all-normal-dispersion femtosecond pulse generation from a Yb-doped large-mode area microstructure fiber laser. Optics Letters, 32(18), 2738-2740.

[44] Isomaki, A., Vainionpaa, A. M., Lyytikainen, J., & Okhotnikov, O. G. (2003). Semiconductor mirror for optical noise suppression and dynamic dispersion compensation. Quantum Electronics, IEEE Journal of, 39(11), 1481-1485.

[45] Okhotnikov, O., Grudinin, A., & Pessa, M. (2004). Ultra-fast fibre laser systems based on SESAM technology: new horizons and applications. New Journal of Physics, 6(177), 1-

[46] Burr, E., Pantouvaki, M., Fice, M., Gwilliam, R., Krysa, A., Roberts, J., & Seeds, A. (2006). Signal stability in periodically amplified fiber transmission systems using multiple quantum well saturable absorbers for regeneration. Journal of Lightwave Technology, 24(2), 747.

[47] Gong, M., Yu, H., Wushouer, X., & Yan, P. (2008). Passively mode-locked Nd: YVO4 picosecond laser with oblique incidence on SESAM. Laser Physics Letters, 5(7), 514-517.

[48] Li, L., Liu, 1. J., Liu, 1. M., Liu, S., Chen, F., Wang, W., & Wang, Y. (2009). 532 nm continuous wave mode-locked Nd: GdVO4 laser with SESAM. Laser Physics Letters, 6(2), 113-116.

[49] Gomes, L. A., Orsila, L., Jouhti, T., & Okhotnikov, O. G. (2004). Picosecond SESAM-based ytterbium mode-locked fiber lasers. Selected Topics in Quantum Electronics, IEEE Journal of, 10(1), 129-136.

[50] Cai, Y., Zhou, C., Zhang, M., Ren, L., Chen, L. L., Kong, W. P., Pang, D. Q., & Zhang, Z. G. (2009). Femtosecond Er doped fiber laser using high modulation depth SESAM based on metal/dielectric hybrid mirror. Laser Physics, 19(10), 2023-2026.

[51] Song, R., Chen, H. W., Chen, S. P., Hou, J., & Lu, Q. S. (2011). A SESAM passively mode-locked fiber laser with a long cavity including a band pass filter. Journal of Optics, 13(3), 035201.

[52] Liu, J., Xu, J., & Wang, P. (2012). High repetition-rate narrow bandwidth SESAM mode-locked Yb-doped fiber lasers. Photonics Technology Letters, IEEE, 24(7), 539-541.

[53] Miller, J. M. (2011). Optimizing and Applying Graphene as a Saturable Absorber for Generating Ultrashort Pulses (Doctoral dissertation, University of Colorado).

[54] Wood, R. M. (2003). Laser-induced Damage of Optical Materials. CRC Press.

[55] Yamashita, S. (2012). A tutorial on nonlinear photonic applications of carbon nanotube and graphene. Lightwave Technology, Journal of, 30(4), 427-447.

[56] Keller, U. (2003). Recent developments in compact ultrafast lasers. Nature, 424(6950), 831-838.

[57] Xiang, N., Guina, M. D., Vainionpaa, A. M., Lyytikainen, J., Suomalainen, S., Saarinen, M. J., Okhotnikov, O., Sajavaara, T., & Keinonen, J. (2002). Broadband semiconductor saturable absorber mirrors in the 1.55-μm wavelength range for pulse generation in fiber lasers. Quantum Electronics, IEEE Journal of, 38(4), 369-374.

[58] Grawert, F. J., Gopinath, J. T., Ilday, F. Ö., Shen, H. M., Ippen, E. P., Kaertner, F. X., Akiyama, S., Liu, J., Wada, K., & Kimerling, L. C. (2005). 220-fs erbiumytterbium: glass laser mode locked by a broadband low-loss silicon/germanium saturable absorber. Optics Letters, 30(3), 329-331.

[59] Popa, D., Sun, Z., Hasan, T., Torrisi, F., Wang, F., & Ferrari, A. C. (2011). Graphene Q-switched, tunable fiber laser. Applied Physics Letters, 98(7), 073106-073106.

[60] Wang, F., Rozhin, A. G., Scardaci, V., Sun, Z., Hennrich, F., White, I. H., Milne, W. I., & Ferrari, A. C. (2008). Wideband-tuneable, nanotube mode-locked, fibre laser. Nature Nanotechnology, 3(12), 738-742.

[61] Guo, T., Nikolaev, P., Thess, A., Colbert, D. T., & Smalley, R. E. (1995). Catalytic growth of single-walled manotubes by laser vaporization. Chemical Physics Letters, 243(1), 49-54.

[62] Dai, H., Rinzler, A. G., Nikolaev, P., Thess, A., Colbert, D. T., & Smalley, R. E. (1996). Single-wall nanotubes produced by metal-catalyzed disproportionation of carbon monoxide. Chemical Physics Letters, 260(3), 471-475.

[63] Journet, C., Maser, W. K., Bernier, P., Loiseau, A., De La Chapelle, M. L., Lefrant, D. L. S., Loiseau, A., Deniard, P., Lee, R., & Fischer, J. E. (1997). Large-scale production of single-walled carbon nanotubes by the electric-arc technique. Nature, 388(6644), 756-758.

[64] Satishkumar, B. C., Govindaraj, A., Sen, R., & Rao, C. N. R. (1998). Single-walled nanotubes by the pyrolysis of acetylene-organometallic mixtures. Chemical Physics Letters, 293(1), 47-52.

[65] Kashiwagi, K., & Yamashita, S. (2010). Optical Deposition of Carbon Nanotubes for Fiber-based Device Fabrication.

[66] Yamashita, S., Inoue, Y., Maruyama, S., Murakami, Y., Yaguchi, H., Jablonski, M., & Set, S. Y. (2004). Saturable absorbers incorporating carbon nanotubes directly synthesized onto substrates and fibers and their application to mode-locked fiber lasers. Optics Letters, 29(14), 1581-1583.

[67] Sakakibara, Y., Rozhin, A. G., Kataura, H., Achiba, Y., & Tokumoto, M. (2005). Carbon nanotube-poly (vinylalcohol) nanocomposite film devices: Applications for femtosecond fiber laser mode lockers and optical amplifier noise suppressors. Japanese Journal of Applied Physics, 44(4), 1621-1625.

[68] Rozhin, A. G., Sakakibara, Y., Namiki, S., Tokumoto, M., Kataura, H., & Achiba, Y. (2006). Sub-200-fs pulsed erbium-doped fiber laser using a carbon nanotubepolyvinylalcohol mode locker. Applied Physics Letters, 88(5), 051118-051118.

[69] Scardaci, V., Sun, Z., Wang, F., Rozhin, A. G., Hasan, T., Hennrich, F., White, I. H., Milne, W. I., & Ferrari, A. C. (2008). Carbon nanotube polycarbonate composites for ultrafast lasers. Advanced Materials, 20(21), 4040-4043.

[70] Gerosa, R. M., Steinberg, D., Rosa, H. G., Barros, C., de Matos, C. J. S., & de Souza, E. A. T. (2013). CNT Film Fabrication for Mode-Locked Er-Doped Fiber Lasers: The Droplet Method. IEEE Photonics Technology Letters, 25(11), 1007-1010.

[71] Nicholson, J. W., Windeler, R. S., & DiGiovanni, D. J. (2007). Optically driven deposition of single-walled carbon-nanotube saturable absorbers on optical fiber end-faces. Optics Express, 15(15), 9176-9183.

[72] Martinez, A., Fuse, K., Xu, B., & Yamashita, S. (2010). Optical deposition of graphene and carbon nanotubes in a fiber ferrule for passive mode-locked lasing. Optics Express, 18(22), 23054-23061.

[72] Set, S. Y., Yaguchi, H., Tanaka, Y., & Jablonski, M. (2004). Ultrafast fiber pulsed lasers incorporating carbon nanotubes. Selected Topics in Quantum Electronics, IEEE Journal of, 10(1), 137-146.

[73] Set, S. Y., Yaguchi, H., Tanaka, Y., & Jablonski, M. (2004). Laser mode locking using a saturable absorber incorporating carbon nanotubes. Journal of Lightwave Technology, 22(1), 51-56.

[74] Jost, O., Gorbunov, A. A., Pompe, W., Pichler, T., Friedlein, R., Knupfer, M., Reibold, M., Bauer, H. D., Dunsch, L., Golden, M. S., & Fink, J. (1999). Diameter grouping in bulk samples of single-walled carbon nanotubes from optical absorption spectroscopy. Applied Physics Letters, 75(15), 2217-2219.

[75] Zheng, M., Jagota, A., Strano, M. S., Santos, A. P., Barone, P., Chou, S. G., Diner, B. A., Dresselhaus, M. S., McLean, R. S., Onoa, G. B., Samsonidze, G. G., Semke, E. D., Usrey, M., & Walls, D. J. (2003). Structure-based carbon nanotube sorting by sequence-dependent DNA assembly. Science, 302(5650), 1545-1548.

[76] Kataura, H., Kumazawa, Y., Maniwa, Y., Umezu, I., Suzuki, S., Ohtsuka, Y., & Achiba, Y. (1999). Optical properties of single-wall carbon nanotubes. Synthetic Metals, 103(1), 2555-2558.

[77] Sun, Z., Hasan, T., Torrisi, F., Popa, D., Privitera, G., Wang, F., Bonaccorso, F., Basko, D. M., & Ferrari, A. C. (2010). Graphene mode-locked ultrafast laser. Acs Nano, 4(2), 803-810.

[78] Going, R., Popa, D., Torrisi, F., Sun, Z., Hasan, T., Wang, F., & Ferrari, A. C. (2012). 500 fs wideband tunable fiber laser mode-locked by nanotubes. Physica E: Low-Dimensional Systems and Nanostructures, 44(6), 1078-1081.

[79] Chamorovskiy, A. Y., Marakulin, A. V., Kurkov, A. S., & Okhotnikov, O. G. (2012). Tunable Ho-doped soliton fiber laser mode-locked by carbon nanotube saturable absorber. Laser Physics Letters, 9(8), 602-606.

[80] Qin, G., Suzuki, T., & Ohishi, Y. (2010). Widely tunable passively mode-locked fiber laser with carbon nanotube films. Optical Review, 17(3), 97-99.

[81] Zhang, H., Tang, D., Knize, R. J., Zhao, L., Bao, Q., & Loh, K. P. (2010). Graphene mode locked, wavelength-tunable, dissipative soliton fiber laser. Applied Physics Letters, 96(11), 111112-111112.

[82] Novoselov, K. S., Geim, A. K., Morozov, S. V., Jiang, D., Zhang, Y., Dubonos, S. V., Grigorieva, I. V., & Firsov, A. A. (2004). Electric field effect in atomically thin carbon films. Science, 306(5696), 666-669.

[83] Bonaccorso, F., Sun, Z., Hasan, T., & Ferrari, A. C. (2010). Graphene photonics and optoelectronics. Nature Photonics, 4(9), 611-622.

[84] Bao, Q., Zhang, H., Wang, Y., Ni, Z., Yan, Y., Shen, Z. X., Loh, K. P., & Tang, D. Y. (2009). Atomic-layer graphene as a saturable absorber for ultrafast pulsed lasers. Advanced Functional Materials, 19(19), 3077-3083.

[85] Kumar, S., Anija, M., Kamaraju, N., Vasu, K. S., Subrahmanyam, K. S., Sood, A. K., & Rao, C. N. R. (2009). Femtosecond carrier dynamics and saturable absorption in graphene suspensions. Applied Physics Letters, 95(19), 191911-191911.

[86] Sun, Z., Popa, D., Hasan, T., Torrisi, F., Wang, F., Kelleher, E. J., Travers, J. C., Nicolosi, V., & Ferrari, A. C. (2010). A stable, wideband tunable, near transformlimited, graphene-mode-locked, ultrafast laser. Nano Research, 3(9), 653-660.

[87] Lee, C. C., Schibli, T. R., Acosta, G., & Bunch, J. S. (2010). Ultra-short optical pulse generation with single-layer graphene. Journal of Nonlinear Optical Physics & Materials, 19(04), 767-771.

[88] Vasko, F. T. (2010). Saturation of interband absorption in graphene. Physical Review B, 82(24), 245422.

[89] Xing, G., Guo, H., Zhang, X., Sum, T. C., & Huan, C. H. A. (2010). The Physics of ultrafast saturable absorption in graphene. Optics Express, 18(5), 4564-4573.

[90] Zhang, H., Tang, D. Y., Zhao, L. M., Bao, Q. L., Loh, K. P., Lin, B., & Tjin, S. C. (2010). Compact graphene mode-locked wavelength-tunable erbium-doped fiber lasers: from all anomalous dispersion to all normal dispersion. Laser Physics Letters, 7(8), 591-596.

[91] Zhang, H., Tang, D. Y., Zhao, L. M., Bao, Q. L., & Loh, K. P. (2009). Large energy mode locking of an erbium-doped fiber laser with atomic layer graphene. Optics Express, 17(20), 17630-17635.

[92] Song, Y. W., Jang, S. Y., Han, W. S., & Bae, M. K. (2010). Graphene mode-lockers for fiber lasers functioned with evanescent field interaction. Applied Physics Letters, 96(5), 051122-051122.

[93] Geim, A. K., & Novoselov, K. S. (2007). The rise of graphene. Nature materials, 6(3), 183-191.

[94] Bao, Q., Zhang, H., Ni, Z., Wang, Y., Polavarapu, L., Shen, Z. X., Xu, Q. H., Tang, D. Y., & Loh, K. P. (2011). Monolayer graphene as a saturable absorber in a mode locked laser. Nano Research, 4(3), 297-307.

[95] Zhao, L. M., Tang, D. Y., Zhang, H., Wu, X., Bao, Q., & Loh, K. P. (2010). Dissipative soliton operation of an ytterbium-doped fiber laser mode locked with atomic multilayer graphene. Optics Letters, 35(21), 3622-3624.

[96] Seibert, K., Cho, G. C., Kütt, W., Kurz, H., Reitze, D. H., Dadap, J. I., Ahn, H., Downer, M. C., & Malvezzi, A. M. (1990). Femtosecond carrier dynamics in graphite. Physical Review B, 42(5), 2842.

[97] Sun, D., Wu, Z. K., Divin, C., Li, X., Berger, C., de Heer, W. A., First, P. N., & Norris, T. B. (2008). Ultrafast relaxation of excited Dirac fermions in epitaxial graphene using optical differential transmission spectroscopy. Physical Review Letters, 101(15), 157402.

[98] Breusing, M., Ropers, C., & Elsaesser, T. (2009). Ultrafast carrier dynamics in graphite. Physical Review Letters, 102(8), 086809.

[99] Casiraghi, C., Hartschuh, A., Lidorikis, E., Qian, H., Harutyunyan, H., Gokus, T., Novoselov, K. S., & Ferrari, A. C. (2007). Rayleigh imaging of graphene and graphene layers. Nano Letters, 7(9), 2711-2717.

[100] Nair, R. R., Blake, P., Grigorenko, A. N., Novoselov, K. S., Booth, T. J., Stauber, T., Peres, N. M. R., & Geim, A. K. (2008). Fine structure constant defines visual transparency of graphene. Science, 320(5881), 1308-1308.

[101] Dawlaty, J. M., Shivaraman, S., Chandrashekhar, M., Rana, F., & Spencer, M. G. (2008). Measurement of ultrafast carrier dynamics in epitaxial graphene. Applied Physics Letters, 92, 042116.

[102] Kumar, S., Anija, M., Kamaraju, N., Vasu, K. S., Subrahmanyam, K. S., Sood, A. K., & Rao, C. N. R. (2009). Femtosecond carrier dynamics and saturable absorption in graphene suspensions. Applied Physics Letters, 95(19), 191911-191911.

[103] Popa, D., Sun, Z., Hasan, T., Torrisi, F., Wang, F., & Ferrari, A. C. (2011). Graphene Q-switched, tunable fiber laser. Applied Physics Letters, 98(7), 073106-073106.

[104] Ahmad, H., Zulkifli, M. Z., Muhammad, F. D., Zulkifli, A. Z., & Harun, S. W. (2013). Tunable graphene-based Q-switched erbium-doped fiber laser using fiber Bragg grating. Journal of Modern Optics, 60(3), 202-212.

[105] Novoselov, K. S., Jiang, D., Schedin, F., Booth, T. J., Khotkevich, V. V., Morozov, S. V., & Geim, A. K. (2005). Two-dimensional atomic crystals. Proceedings of the National Academy of Sciences of the United States of America, 102(30), 10451-10453.

[106] Obraztsov, A. N., Obraztsova, E. A., Tyurnina, A. V., & Zolotukhin, A. A. (2007). Chemical vapor deposition of thin graphite films of nanometer thickness. Carbon, 45(10), 2017-2021.

[107] Reina, A., Jia, X., Ho, J., Nezich, D., Son, H., Bulovic, V., Dresselhaus, M. S., & Kong, J. (2008). Large area, few-layer graphene films on arbitrary substrates by chemical vapor deposition. Nano Letters, 9(1), 30-35.

[108] Vlassiouk, I., Fulvio, P., Meyer, H., Lavrik, N., Dai, S., Datskos, P., & Smirnov, S. (2013). Large scale atmospheric pressure chemical vapor deposition of graphene. Carbon, 54, 58–67.

[109] Zhang, Y., Zhang, L., & Zhou, C. (2013). Review of Chemical Vapor Deposition of Graphene and Related Applications. Accounts of chemical research.

[110] Hernandez, Y., Nicolosi, V., Lotya, M., Blighe, F. M., Sun, Z., De, S., McGovern, I. T., Holland, B., Byrne, M., Gun'Ko, Y. K., Boland, J. J., Niraj, P., Duesberg, G., Krishnamurthy, S., Goodhue, R., Hutchison, J., Scardaci, V., Ferrari, A. C., & Coleman, J. N. (2008). High-yield production of graphene by liquid-phase exfoliation of graphite. Nature Nanotechnology, 3(9), 563-568.

[111] Lotya, M., Hernandez, Y., King, P. J., Smith, R. J., Nicolosi, V., Karlsson, L. S., Blighe, F. M., De, S., Wang, Z., McGovern, I. T., Duesberg, G. S., & Coleman, J. N. (2009). Liquid phase production of graphene by exfoliation of graphite in surfactant/water solutions. Journal of the American Chemical Society, 131(10), 3611-3620.

[112] BittoloáBon, S. (2011). High concentration few-layer graphene sheets obtained by liquid phase exfoliation of graphite in ionic liquid. Journal of Materials Chemistry, 21(10), 3428-3431.

[113] Choucair, M., Thordarson, P., & Stride, J. A. (2008). Gram-scale production of graphene based on solvothermal synthesis and sonication. Nature Nanotechnology, 4(1), 30-33.

[114] Eigler, S., Enzelberger-Heim, M., Grimm, S., Hofmann, P., Kroener, W., Geworski, A., Dotzer, C., Röckert, M., Xiao, J., Papp, C., Lytken, O., Steinrück, H. P., Müller, P., & Hirsch, A. (2013). Wet chemical synthesis of graphene. Advanced Materials, 25(26), 3583–3587.

[115] Mohsin, D. Schall, M. Otto, A. Noculak, D. Neumaier, and H. Kurz, "Graphene based low insertion loss electro-absorption modulator on SOI waveguide," Opt. Express 22, 15292-15297 (2014).

[116] Q. Bao, H. Zhang, Y. Wang, Z. Ni, Y. Yan, Z. X. Shen, K. P. Loh, and D. Y. Tang, "Atomic-layer graphene as a saturable absorber for ultrafast pulsed lasers," Advanced Functional Materials, vol. 19, no. 19, pp. 3077–3083, 2009.

[117] Alexander, Koen, Bart Kuyken, and Dries Van Thourhout. 2016. "Characterization of Graphene-covered SiN Waveguide Using Four-wave Mixing." In , 61–64.

[118] "www.graphenea.com," 2016.

[119] K. Alexander, Y. Hu, M. Pantouvaki, S. Brems, I. Asselberghs, S. Gorza, C. Huyghebaert, J. Van Campenhout, B. Kuyken, and D. Van Thourhout, "Electrically Controllable Saturable Absorption in Hybrid Graphene-Silicon Waveguides," in CLEO: 2015, OSA Technical Digest (online) (Optical Society of America, 2015), paper STh4H.7.

[120] N. W. Ashcroft et al. Solid State Physics. Brooks/Cole, Belmont, California, 1976.

[121] "www.thephysicsmill.com/2013/02/03/im-with-the-valence-band-band-structure-and-the-science-of-conduction/", 2017

[122] Dries Van Thourhout Koen Alexander, N. A. Savostianova, S. A. Mikhailov, Bart Kuyken, “Electrically Tunable Optical Nonlinearities in Graphene-Covered SiN Waveguides Characterized by Four-Wave Mixing”, arxiv.org, arXiv:1704.08567v2

[123] https://arxiv.org/ftp/arxiv/papers/1101/1101.4383.pdfwave

[124] Gautam, Deepraj, Dries Van Thourhout, and Lukas Novotny [ETH Zurich]. Electrically Switchable Four Wave Mixing In Graphene. Master of Science in Photonics Engineering.

[125] http://www.photonics.intec.ugent.be/research/topics.asp?ID=161

[126] A. Marini, J. D. Cox, and F. J. García de Abajo, “Theory of graphene saturable absorption”, Phys. Rev. B 95, 125408 – Published 6 March 2017

Annexes

Annex I

Code used for getting data in order to characterize chip waveguides:

```
import numpy as np
from pymeasure.units.unit import NANOMETER, PICOMETER,
                                 MILLISECOND, DBM, SECOND, MILLIWATT
from pymeasure.instruments.Santec.tunable_laser import
                                                 SantecTunableLaserTSL510
from pymeasure.instruments.HP.power_meter import
                                                       HPPowerMeter8153A
import pylab as pl
import csv
import time
def example():
    name='53st_W2200_L100_1'
    wls=np.arange(1500, 1630, 1)
    #  initialize instruments
    L = SantecTunableLaserTSL510( name = "Santec Laser", address
                                                 = "GPIB::25")
    L.power = 10*DBM
    L.wavelenth = wls[0]
    PM = HPPowerMeter8153A( name = "HP 8153A Powermeter",
                                    address = "GPIB::30")
    PM.initialize()
    PM.channel='B'
    PM.wavelength = 1550 * NANOMETER
    PM.averaging_time = 100 * MILLISECOND
    PM.range = 'AUTO'
    PM.power_unit = DBM
    PM.channel='A'
    PM.wavelength = 1550 * NANOMETER
    PM.averaging_time = 100 * MILLISECOND
    PM.range = 'AUTO'
    PM.power_unit = DBM
    powers=np.zeros(np.size(wls))
    i=0
    for wl in wls:
      print wl
      L.current_frequency = wl * NANOMETER
      L.wavelenth = wl
      time.sleep(0.2)
      powers[i] = PM.get_power().get_value()
      i=i+1
    pl.plot(wls, powers,'-')
    pl.xlabel('Wavelength (nm)')
    pl.ylim(-55, -10)
    pl.ylabel('Transmitted power (dBm)')
    pl.grid(True)
    pl.savefig(name+'.png')
    pl.show()
    pl.clf()
    with open(name+'.csv', 'wb') as csvfile:
          writer = csv.writer(csvfile, delimiter='\t')
          i=0
          for wl in wls:
                writer.writerow([wl, powers[i]])
                i=i+1
example()
```

Annex II

Code used to process data for waveguide characterization:

```
import pylab
import os
import numpy as np
import matplotlib.pyplot as plt
import matplotlib.patches as mpatches
from os import listdir
from os.path import isfile, join
import csv

path="C:\Users\Miguel\Desktop\TFM_Gent_24_05_2017\Mesurements\se
      tup 10 Horizontal_Santec"
norm_file = 'normalizationF2F.csv'
W=1200.0
L=[50, 100, 200, 400, 800]

def Plotear(x, y, figura="", Titulo="", ColorPlot='b',
            Marcador='None', TipoPlot="-", Etiqueta=None,
            LocEtiqueta=(0.10, 0.1), xlabel='xxlabel',
            ylabel='yylabel', orden=None):
    plt.ioff()
    fig=plt.figure(figura)
    plt.suptitle(Titulo)

    if Etiqueta!=None:
        red_patch = mpatches.Patch(color=ColorPlot,
                        label=Etiqueta)
        plt.legend(bbox_to_anchor=LocEtiqueta, loc=2,
                        borderaxespad=0, handles=[red_patch])

    plt.plot(x, y, color=ColorPlot, linestyle=TipoPlot,
                    zorder=orden, marker=Marcador)
    ax = fig.add_subplot(1,1,1)

    plt.tick_params(which='major', width=2, length=10,
                        direction='out')
    plt.tick_params(which='minor', width=1, length=5,
                        direction='out')

    #and a corresponding grid
    ax.grid(which='both')
    # or if you want differnet settings for the grids:
    ax.grid(which='minor', alpha=0.1)
    ax.grid(which='major', alpha=0.5)
    ax.get_yaxis().get_major_formatter().set_useOffset(False)
    plt.ylabel(ylabel)
    plt.xlabel(xlabel)


def takeData():
    os.chdir(path)  # Set the path where are the mesurements
    mypath = os.getcwd()
    onlyfiles = [f for f in listdir(mypath) if
                    isfile(join(mypath, f))]

    #take the normalization data
    wavelength=[]
    pot_norm=[]
    with open(norm_file, 'rb') as csvfile:
```

```
        reader = csv.reader(csvfile, dialect='excel', delimit
            ter='\t')
        for row in reader:
            wavelength.append(float(row[0]))
            pot_norm.append(float(row[1]))

    data_all = np.zeros((len(L), len(wavelength)))
    for i in range(len(L)):  #for each length of graphene
        filensearched = "_W" + str(int(W)) + "_L" +
                            str(int(L[i]))
        for file in onlyfiles: #search in all files
            if file.endswith('.csv')==True and (filensearched in
                                                    file)==True:
                #Take data from files
                with open(file, 'rb') as csvfile:
                    reader = csv.reader(csvfile,
                                        dialect='excel',
                                        delimiter='\t')
                    count=0
                    for row in reader:
                        data_all[i][count] = float(row[1]) -
                                                    pot_norm[count]
                        count+=1
    return data_all, wavelength


def alpha(lamb):
    data, wavelengths = takeData()
    power = []
    count = 0
    for i in range(np.shape(data)[0]):  # for each length
        count = 0
        for j in range(np.shape(data)[1]):
            if (wavelengths[j] < lamb):
                count += 1

        Xo = wavelengths[count - 1]
        Yo = data[i][count - 1]
        X1 = wavelengths[count]
        Y1 = data[i][count]
        X = lamb
        Y = Yo + (X - Xo) * ((Y1 - Yo) / (X1 - Xo)) #Linear int.
        power.append(Y)

    coef = np.polyfit(L, power, 1)
    alpha = coef[0]
    axis_cut = coef[1]

    '''#Print data
    Lextend=L[:]
    Lextend.extend([-50, 850])
    yfit=[]
    for i in range(len(Lextend)):
        yfit.append(axis_cut+alpha*Lextend[i])

    Plotear(L, power)
    Plotear(Lextend, yfit, TipoPlot='--', ColorPlot='r',
                Etiqueta='alpha= ' + str(alpha), Titulo=str(lamb)+'nm
                '+ ' and  W= '+ str(W)+'nm', xlabel='L',
                ylabel='dBm')
    plt.plot(L,power, 'ro')
```

```
    plt.show()'''

    return alpha, axis_cut

def alpha2(lamb):
    data, wavelengths = takeData()
    power = []
    count = 0
    for i in range(np.shape(data)[0]):  # for each length
        count = 0
        for j in range(np.shape(data)[1]):
            if (wavelengths[j] < lamb):
                count += 1

        Xo = wavelengths[count - 1]
        Yo = data[i][count - 1]
        X1 = wavelengths[count]
        Y1 = data[i][count]
        X = lamb
        Y = Yo + (X - Xo) * ((Y1 - Yo) / (X1 - Xo)) #Linear int.
        power.append(Y)

    power2=[-17.4, -18.9, -23.6, -38.2, -46.8] #for W=1200
    #power2 = [-17.1, -24.0, -14.8, -50.8, -56.0]  # for W=1400

    coef = np.polyfit(L, power, 1)
    coef2 = np.polyfit(L, power2, 1)

    alpha = coef[0]
    alpha2 = coef2[0]
    axis_cut = coef[1]
    axis_cut2 = coef2[1]

    #Print data
    Lextend=L[:]
    Lextend.extend([-50, 850])
    yfit=[]
    yfit2 = []
    for i in range(len(Lextend)):
        yfit.append(axis_cut+alpha*Lextend[i])
        yfit2.append(axis_cut2 + alpha2 * Lextend[i])

    Plotear(L, power)
    Plotear(L, power2, ColorPlot='r')
    Plotear(Lextend, yfit, TipoPlot='--', ColorPlot='b')
    Plotear(Lextend, yfit2, TipoPlot='--', ColorPlot='r',
                Etiqueta='alpha= ' + str(alpha) + '  alpha2= ' +
                str(alpha2),
                Titulo=str(lamb) + 'nm ' + ' and  W= ' + str(W) +
                'nm', xlabel='L', ylabel='dBm')
    plt.plot(L,power, 'bo')
    plt.plot(L, power2, 'ro')
    plt.show()

    return alpha, axis_cut, alpha2, axis_cut2,

def grapheneLosses(): #shape for each lambda
    wavelengths = np.linspace(1500.0, 1629.0, 100)
    alphas = []
    for i in range(len(wavelengths)):
        alphas.append(alpha(wavelengths[i])[0])
```

```
    Plotear(wavelengths, alphas, xlabel='nm', ylabel='dB/um',
                  Titulo='W='+str(W)+'nm' )
    plt.show()


def couplingLosses(): #cuts with 0 for each lambda
    wavelengths = np.linspace(1500.0, 1629.0, 100)
    axis_cuts = []
    for i in range(len(wavelengths)):
        axis_cuts.append(alpha(wavelengths[i])[1])

    Plotear(wavelengths, axis_cuts , Titulo='W='+str(W)+'nm' ,
                  xlabel='nm', ylabel='dBm')
    x_cut2=alpha2(1550)[3]
    x_cut2_array= np.ones(len(wavelengths))*x_cut2
    plt.plot(wavelengths, x_cut2_array, 'r')
    plt.show()

    ''''# Save data
    filename = "GrattingLosses_W_"+str(W)[: 4] + ".txt"
    outfile = open(filename,'w')
    counter = 0
    for wl in wavelengths:
       print >> outfile, wl, axis_cuts[counter]
       outfile.flush()
       counter = counter + 1
    outfile.close'''

#print alpha2(1550)
#grapheneLosses()
#couplingLosses()
```

Annex III

Code used to measure saturable absorption. Basically takes data from channel A and B periodically, get the transmitivity and then save data in a text file.

```
from pymeasure.instruments.Syntune import *
import time
import pylab as pl
import csv

def example():
    wls = 1549.0
    name = "gatting_3er_shortWaveguides_Left_200mA_Voltage_0mV"
    numPoints = 800

    Lg=12.0
    #Lg=8.3
    L_PC=0.6
    divisor=90

    #  initialize instruments
     PM = HPPowerMeter8153A(name="HP 8153A Powermeter",
                            address="GPIB::30")
    PM.initialize()
    PM.wavelength = 1549 * NANOMETER
    PM.averaging_time = 100 * MILLISECOND
    PM.range = 'AUTO'
    PM.channel = 'A'
    PM.power_unit = DBM
    PM.averaging_time = 0.05 * SECOND
    PM.channel = 'B'
    PM.range = 'AUTO'
    PM.power_unit = DBM
    PM.averaging_time = 0.05 * SECOND

    powersA = np.zeros(numPoints)
    powersB= np.zeros(numPoints)
    for j in range(numPoints):
        PM.channel = 'A'
        powersA[j] = PM.get_power().get_value()
        PM.channel = 'B'
        powersB[j] = PM.get_power().get_value()
        print 'iteration ' + str(j) + '/' + str(numPoints) + "
                  move"
        time.sleep(0.2) #time in seconds

    peaks=np.zeros(numPoints)
    T=np.zeros(numPoints)

    for i in range(numPoints):
        #peaks[i] = 10*np.log10(divisor/(100-divisor)) +
                        powersB[i] - Lg + L_PC
        peaks[i] = 8.78 + powersB[i] - Lg + L_PC #experimentally
        T[i] = (powersA[i] + Lg) - peaks[i]
        #T[i] = ( powersB[i]+Lg) - ( 10*np.log10(divisor/(100-
                  divisor)) + powersA[i] - Lg )

    pl.scatter(peaks, T)
    pl.xlabel('peak power input')
    pl.ylabel('Transmitted power (dB)')
    pl.grid(True)
    pl.show()
```

```
    pl.scatter(peaks, T)
    pl.xlabel('average power input')
    pl.ylabel('Transmitted power (dB)')
    pl.grid(True)
    pl.axis([-40, -5, -10, 0])
    pl.savefig(name + '.png')
    pl.clf()

    with open(name + '.csv', 'wb') as csvfile:
        writer = csv.writer(csvfile, delimiter='\t')
        k = 0
        for k in range(numPoints):
            writer.writerow([powersA[k], powersB[k], peaks[k],
                             T[k]])
            k = k + 1

example()
```

Annex IV

Code used to process data when averaging in stretches and gating graphene.

```
import numpy as np
import matplotlib
import matplotlib.pylab as pl
import csv
import matplotlib.colors
import matplotlib.cm as cm
from scipy.optimize import curve_fit

window=3.0  #dB at the x-axis
Lg=11.2 #dB losses of the gratting coupler
L_PC = 0.6 #dB losses of the polarization controller and the
            piece of cable to the gratting

def readfile(filename):
    T=[]
    inputpower=[]
    DA=[]
    DB=[]
    with open(filename, 'rb') as csvfile:
        reader=csv.reader(csvfile, dialect='excel',
                          delimiter='\t')
        for row in reader:
            DA.append(float(row[0]))
            DB.append(float(row[1]))
            inputpower.append(float(row[2]))
            T.append(float(row[3]))
    return DA, DB, inputpower, T

def quiterrors(data, weigth):  #we can asume data in dB
    mean = np.mean(data)
    thresholdUp = mean + weigth
    thresholdDown = mean - weigth
    for i in range(len(data)):
        if data[i]> thresholdUp:
            data[i] = mean
        elif data[i]<thresholdDown:
            data[i] = mean
    return data

def order(x, y):
  n=len(x)
  for i in range(0, n - 1):
      k = i
      t = x[i]
      for j in range(i, n):
          if x[j] <= t:
              k = j
              t = x[j]
              t_y=y[j]
      x[k] = x[i]
      y[k] = y[i]
      x[i] = t
      y[i] = t_y
  return x, y

def smoothing(x, y):
    x_windows = np.arange(round(min(x))-window/2.0,
                          max(x)+window/2.0, window)
```

```
    x_axis = np.arange(round(min(x)), max(x)+window, window)
    means=[]
    typdev=[]
    for i in x_windows:
        segment = []
        for j in range(len(x)):
            if x[j]>=i and x[j]<i+window :
                segment.append(y[j])
        if segment==[]:
            index=np.where(x_axis==i+window/2.0)
            x_axis=np.delete(x_axis, index)
        else:
            segment=quiterrors(segment, 4.0)
            means.append(np.mean(segment))
            typdev.append(np.std(segment))

    return x_axis, means, typdev

def onePlot():
    fichero="pulsed_12LastShortLeftWaveguide_90_10_200mA.csv"
    DB, DA, inputpower, T_measuring = readfile(fichero)

    Trans = np.zeros(len(DA))
    Pinput_avg = np.zeros(len(DA))
    for i in range(len(DA)):
        # Pinput_avg[i] = 10*np.log10(divisor/(100-divisor)) +
                                                    DB[i] - Lg - PC
        Pinput_avg[i] = 8.78 + DB[i] - Lg - L_PC #experimentally
        Trans[i] = (DA[i] + Lg) - Pinput_avg[i]
    #T_order, inPower_order = order(Pinput_avg, Trans) #not need
    x_axis, means, typdev = smoothing(Pinput_avg, Trans)

    fig, ax = pl.subplots()
    #ax.plot(x_axis, means, 'r-*', label='Fitted')
    #ax.plot(x_axis, typdev, 'g-*', label='Fitted')
    ax.errorbar(x_axis, means, yerr=typdev, fmt='r-o',
                label='Fitted')
    ax.scatter(Pinput_avg, Trans, color='skyblue',
                label='Measured')
    ax.set_xlabel('Average Input Power (dBm)')
    ax.set_ylabel('Average Transmission Power (dB)')
    ax.grid()
    pl.show()

def gatingPlots():
    #voltages = ['0V', 'neg100mV', 'neg200mV', 'neg400mV',
                # 'neg600mV', 'neg800mV', 'neg1000mV',
                # 'neg1200mV', 'pos100mV', 'pos200mV',
              # 'pos300mV', 'pos400mV', 'pos500mV']
    voltages = ['0V', 'neg100mV', 'neg200mV', 'neg400mV',
                'neg600mV', 'neg800mV', 'neg1000mV', 'neg1200mV']
    prefix = "gatting_5er_shortWaveguides_Right_200mA_Voltage_"

    fig, ax = pl.subplots(num=None, figsize=(16, 12), dpi=80,
                          facecolor='w', edgecolor='k')
    cmap1 = pl.cm.hot
    cmap2 = pl.cm.cool
    color=0

    for v in voltages:
        filename=prefix + v + '.csv'
```

```
        try:
            DA, DB, inputpower, T_measuring = readfile(filename)

            Trans = np.zeros(len(DA))
            Pinput_avg = np.zeros(len(DA))
            for i in range(len(DA)):
                # Pinput_avg[i] = 10*np.log10(divisor/(100-
                                        divisor)) + DB[i] - Lg - PC
                Pinput_avg[i] = 8.78 + DB[i] - Lg - L_PC
                Trans[i] = (DA[i] + Lg) - Pinput_avg[i]
            x_axis, means, typdev = smoothing(Pinput_avg, Trans)
            if color < 8:
                pl.plot(x_axis, means, '-*', label=v,
                             c=cmap1(color * 20))
                #pl.errorbar(x_axis, means, yerr=typdev, fmt='-
                                    o', label=v)
            else:
                pl.plot(x_axis, means, '-*', label=v,
                             c=cmap2((color - 8) * 100))
                #pl.errorbar(x_axis, means, yerr=typdev, fmt='-
                                    o', label=v)
        except:
            print 'error openning fie: ' + filename
        color += 1

    ax.set_xlabel('Average Input Power (dBm)')
    ax.set_ylabel('Average Transmission Power (dB)')
    ax.set_title(prefix)
    ax.grid(True)
    ax.set_xlim([-40, 0])
    ax.set_ylim([-2, 2])

    pl.legend(bbox_to_anchor=(0.97, 0.75), loc=2,
                                                borderaxespad=0.)
    pl.show()

onePlot()
gatingPlots()
```

Annex V

Code used for fitting saturable absorption data with theoretically derivative equations.

```
import numpy as np
import matplotlib.pylab as pl
import csv
from scipy.optimize import curve_fit
from pylab import *
from mpl_toolkits.mplot3d import Axes3D
import matplotlib.cm as cm

filename="gatting_5er_shortWaveguides_Left_200mA_Voltage_
                                                          0mV.csv"
Lg = 8.3  #losses of gratting coupling
PC = 0.6  #losses of Polarization controller

numPoints = 201  # number of points to calculate the
                        differential equation
L = 100.0  # um -> length of the graphene
powerStep = 0.5

def plotgraph1(x1, y1, x2, y2, type):
    fig, ax = pl.subplots()
    ax.plot(x1, y1, 'ob', label='Fitting')
    ax.plot(x2, y2, type, label='Measured')
    pl.xlabel('Pin (dBm)')
    pl.ylabel('T (dB)')
    pl.title('test')
    pl.grid(True)
    pl.show()

def alpha(P0, Alpha0, A):
    #A=sqrt(P)
    Alpha0_m = Alpha0 / (10.0*np.log10(np.e))
    return Alpha0_m/(1.0+((A**2.0)/P0))

def integral(A0, numPoints, P0, Alpha0, dz):
    A = [A0]
    for i in range(numPoints):
        dA = A[i] - (alpha(P0, Alpha0, A0) / 2.0) * A[i] * dz
        A.append(dA)
    return A[-1]

def loadfile():
    T = []
    inputpower = []
    DA = []
    DB = []
  #Read the file
    with open(filename, 'rb') as csvfile:
        reader = csv.reader(csvfile, dialect='excel',
                                                  delimiter='\t')
        for row in reader:
            DA.append(float(row[0]))
            DB.append(float(row[1]))
            inputpower.append(float(row[2]))
            T.append(float(row[3]))
  #Calculate T and average InputPower
    T_correct = np.zeros(len(DA))
    Pinput_avg = np.zeros(len(DA))
    for i in range(len(DA)):
```

```
        Pinput_avg[i] = 8.78 + DB[i] - Lg - PC
        T_correct[i] = (DA[i] + Lg) - Pinput_avg[i]
    return Pinput_avg, T_correct

def smoothing(x, y):
    x_windows = np.arange(round(min(x))-powerStep/2.0,
                              max(x)+powerStep/2.0, powerStep)
    x_axis = np.arange(round(min(x)), max(x)+powerStep,
                                                          powerStep)
    means=[]
    typdev=[]
    for i in x_windows:
        segment = []
        for j in range(len(x)):
            if x[j]>=i and x[j]<i+powerStep :
                segment.append(y[j])
        if segment==[]:
            index=np.where(x_axis==i+powerStep/2.0)
            x_axis=np.delete(x_axis, index)
        else:
            means.append(np.mean(segment))
            typdev.append(np.std(segment))
    return x_axis, means, typdev

def diffEql(x, P0, Alpha0):
  #Initial values
    dz= L/(numPoints-1) #spacing between points

    #P0 = 0.0  #dBM
    P0 = 10.0**(P0/10.0) * 1e-3  # in Watts

    Pin = np.arange(round(min(x)), max(x) + powerStep,
                        powerStep)
    Pout=[]
    T=[]
    for Pj in Pin:
        A0= np.sqrt( 10.0**(Pj/10.0) * 1e-3)
        Aout=integral(A0, numPoints, P0, Alpha0, dz)
        Pout_aux = (Aout)**2.0  #in wats
        Pout_aux = 30.0 + 10.0*np.log10(Pout_aux) #in dBm
        Pout.append(Pout_aux)  #add value
        T.append(Pout_aux-Pj)

    return Pin, Pout, T



def fittingP0(P0, Alpha0): #P0 -> dBM  #Alpha0 -> dBm/um
    Pinput_meas, T_meas = loadfile()
    x_axis, means, typdev = smoothing(Pinput_meas, T_meas)
    P0_array=np.linspace(P0*0.75, P0*1.25, 50)
    Pin_eq, Pout_eq, T_eq = diffEql(x_axis, P0, Alpha0)
    plotgraph1(Pin_eq, T_eq, x_axis, means, type='-b')
    error = []
    for p in P0_array:
        Pin_eq, Pout_eq, T_eq = diffEql(x_axis, p, Alpha0)
        index_meas=0
        sum_error = 0
        for x in x_axis:
            index_calc=np.where(Pin_eq==x)
            sum_error += ((( means[index_meas] -
```

```
                                T_eq[int(index_calc[0])]))**2)
                index_meas+=1
            error.append(sum_error)
        error_min=min(error)
        index=int(np.where(error==error_min)[0])
        plotgraph1(P0_array, error, x2=P0_array[index],
                      y2=error_min, type='or')
        P0_fit = P0_array[index]
        Pin_eq, Pout_eq, T_eq = diffEql(x_axis, P0_fit, Alpha0)
        plotgraph1(Pin_eq, T_eq, x_axis, means, type='-r')
        return P0_fit, error_min

    def fittingA0(P0, Alpha0): #P0 -> dBM  #Alpha0 -> dBm/um
        Pinput_meas, T_meas = loadfile()
        x_axis, means, typdev = smoothing(Pinput_meas, T_meas)
        Alpha0_array=np.linspace(Alpha0*0.75, Alpha0*1.25, 50)
        Pin_eq, Pout_eq, T_eq = diffEql(x_axis, P0, Alpha0)
        plotgraph1(Pin_eq, T_eq, x_axis, means, type='-b')
        error = []
        for a in Alpha0_array:
            Pin_eq, Pout_eq, T_eq = diffEql(x_axis, P0, a)
            index_meas=0
            sum_error = 0
            for x in x_axis:
                index_calc=np.where(Pin_eq==x)
                sum_error += ((( means[index_meas] -
                                T_eq[int(index_calc[0])]))**2)
                index_meas+=1
            error.append(sum_error)
        error_min=min(error)
        index=int(np.where(error==error_min)[0])
        plotgraph1(Alpha0_array, error, x2=Alpha0_array[index],
                      y2=error_min, type='or')
        Alpha0_fit = Alpha0_array[index]
        Pin_eq, Pout_eq, T_eq = diffEql(x_axis, P0, Alpha0_fit)
        plotgraph1(Pin_eq, T_eq, x_axis, means, type='-r')
        return Alpha0_fit, error_min

    def initial(P0, Alpha0):
        Pinput_meas, T_meas = loadfile()
        x_axis, means, typdev = smoothing(Pinput_meas, T_meas)
        index_meas = 0
        sum_error = 0
        Pin_eq, Pout_eq, T_eq = diffEql(x_axis, P0, Alpha0)
        error = []
        for x in x_axis:  #
            index_calc = np.where(Pin_eq == x)
            sum_error += (((means[index_meas] -
                            T_eq[int(index_calc[0])])) ** 2)
            index_meas += 1
        error.append(sum_error)
        error_min = min(error)
        plotgraph1(Pin_eq, T_eq, x_axis, means, type='-b')
        return error_min

    print initial(P0=0.201, Alpha0=0.05969)
    #print fittingP0(P0=0.201, Alpha0=0.05969)
    #print fittingA0(P0=0.201, Alpha0=0.05969)
```

Annex VI

Lumerical code used obtaing the overlap between coupling and waveguide field .

```
switchtolayout;
deleteall;
clear;
um=10^(-6); #unit
nm=10^(-9); #unit

#_____Silicon Oxide_____#
addrect;
set("name", "Silicon Oxide");
set("x",0);
set("y",-1.8*um);
set("z",0);
set("x span", 20.0*um);
set("y span", 4.0*um);
set("z span", 0);
set("material", "SiO2 (Glass) - Palik");

#_____Silicon Nitride_____#
addrect;
set("name", "Silicon Nitride");
set("x",0);
set("y",0);
set("z",0);
set("x span", 1.2*um);
set("y span", 330*nm);
set("z span", 0);
set("index", 1.9963);

#_____Residual Nitride_____#
addrect;
set("name", "Residual Nitride");
set("x",0);
set("y",-0.15*um);
set("z",0);
set("x span", 20.0*um);
set("y span", 30*nm);
set("z span", 0);
set("index", 1.9963);

#_____Silicon_____#
addrect;
set("name", "Silicon");
set("x",0);
set("y",-5.8*um);
set("z",0);
set("x span", 20.0*um);
set("y span", 4.0*um);
set("z span", 0);
set("material", "Si (Silicon) - Palik");

#__________SOLVER___________#
addfde;
set("x",0);
set("y",2*um);
set("z",0);
set("x span", 18*um);
set("y span", 10*um);
```

```
#set("z span", 10*um); #the requested property is inactive
set("x min BC", "Metal");
set("x max BC", "Metal");
set("y min BC", "Metal");
set("y max BC", "Metal");

#__________MESH___________#
addmesh;
set("name", "FineCenterMesh");
set("x",0);
set("y",2*um);
set("z",0);
set("x span", 18*um);
set("y span", 10*um);
set("z span", 0);
set("dx",0.04*um);
set("dy",0.04*um);

#__________SET ANLAYSIS___________#
setanalysis("number of trial modes", 1);
setanalysis("search", "near n");
setanalysis("use max index", 0);
setanalysis("n", 1.9963);

#__________SET BEAM___________#
setanalysis("use fully vectorial thin lens beam profile", 0);
setanalysis("waist radius", 1.25*um);
setanalysis("sample resolution", 400);
beamname=createbeam;

#__________CHANGE WIDTHS___________#
widths=(100*nm):(50*nm):(1200*nm);

for(x=widths) {
    switchtolayout;
    setnamed("Silicon Nitride","x span", x);
    findmodes;
    out=overlap("mode1", "gaussian1");
    write("sweepLumerical2.txt",num2str(x));
    write("sweepLumerical2.txt",num2str(out(2)));
    run;
}
```